Available online at www.sciencedirect.com

ScienceDirect

Geochimica et Cosmochimica Acta 270 (2020) 264–281

Geochimica et Cosmochimica Acta

www.elsevier.com/locate/gca

On geologic timescales, plant carbon isotope fractionation responds to precipitation similarly to modern plants and has a small negative correlation with pCO_2

Kristen Schlanser [a,*], Aaron F. Diefendorf [a], David R. Greenwood [b], Kevin E. Mueller [c], Christopher K. West [d], Alexander J. Lowe [b,e], James F. Basinger [d], Ellen D. Currano [f], Andrew G. Flynn [g], Henry C. Fricke [h], Jie Geng [g], Herbert W. Meyer [i], Daniel J. Peppe [g]

[a] *Department of Geology, University of Cincinnati, Cincinnati, OH 45221, USA*
[b] *Department of Biology, Brandon University, 270 18th Street, Brandon, MB R7A 6A9, Canada*
[c] *Biological, Geological and Environmental Sciences, Cleveland State University, 2121 Euclid Ave, Cleveland, OH 44115, USA*
[d] *Department of Geological Sciences, University of Saskatchewan, 114 Science Place, Saskatoon, SK S7N 5E2, Canada*
[e] *Department of Biology, University of Washington, 24 Kincaid Hall, Seattle, WA 98195, USA*
[f] *Departments of Botany and Geology & Geophysics, University of Wyoming, 1000 E. University Ave, Laramie, WY 82071, USA*
[g] *Terrestrial Paleoclimatology Research Group, Department of Geosciences, Baylor University, 101 Bagby Ave, TX 76706, USA*
[h] *Geology Department, Colorado College, 14 E. Cache La Poudre, Colorado Springs, CO 80903, USA*
[i] *National Park Service, Florissant Fossil Beds National Monument, Florissant, P.O. Box 185, CO 80816, USA*

Received 9 June 2019; accepted in revised form 19 November 2019; Available online 27 November 2019

Abstract

Leaf carbon isotope fractionation (Δ_{leaf}) is sensitive to environmental conditions and can provide insights into the state and evolution of leaf gas-exchange in response to climate and environment factors. In modern plants, water availability is the strongest environmental predictor of Δ_{leaf} across sites that experience relatively uniform and low concentrations of CO_2 in the atmosphere (pCO_2). Growth chamber experiments show Δ_{leaf} of modern plants can also be sensitive to changing pCO_2. However, over geologic time, it is uncertain how Δ_{leaf} has responded to shifts in pCO_2 and precipitation. To address this problem, we collected sediment (rock) samples from fossil leaf sites that represent a range of pCO_2 values from ~200 to 900 ppmV, over 40 degrees of latitude from New Mexico to the High Arctic, and 40 million years spanning the Late Cretaceous to the Oligocene. For each site, the carbon isotope composition of atmospheric CO_2 ($\delta^{13}C_{atm}$), pCO_2, mean annual precipitation, and mean annual temperature were constrained from independent proxies. From sediment samples, we extracted long-chain *n*-alkanes (biomarkers derived from plant wax). We then measured the carbon isotope ratios of sediment-derived *n*-C_{29} and *n*-C_{31} alkanes to calculate Δ_{leaf}. Results show a negative correlation between Δ_{leaf} and pCO_2 even after controlling for mean annual precipitation. The Δ_{leaf} response to pCO_2 is small (-0.3 ± 0.09‰/100 ppmV), suggesting plants are adjusting internal leaf CO_2 concentrations to atmospheric pCO_2 concentrations, likely by optimizing leaf gas-exchange to maximize carbon intake and minimize water loss in response to environmental conditions. Similar to previous studies of geologic sediments and living plants, Δ_{leaf} was also positively correlated with water availability and, to a lesser extent, sensitive to plant type and

* Corresponding author.
E-mail address: kschlans@gmail.com (K. Schlanser).

https://doi.org/10.1016/j.gca.2019.11.023

possibly altitude. As a result, the $\Delta_{leaf} - pCO_2$ relationship in the geologic past may be more complex than observed in modern studies and therefore, precludes its use as a pCO_2 proxy.

Keywords: *n*-Alkanes; Leaf waxes; Paleogene; Cretaceous; North America; Arctic; Organic geochemistry; Paleobotany; Fossil leaves

1. INTRODUCTION

Leaf carbon isotope fractionation (Δ_{leaf}) in C_3 plants depends partly on how stomata regulate leaf gas-exchange, which helps explain the sensitivity of Δ_{leaf} to a number of environmental and biological factors including water availability and physiological traits (O'Leary, 1981; Körner et al., 1988; Farquhar et al., 1989; Diefendorf et al., 2010; Kohn, 2010; Cernusak et al., 2013; Graham et al., 2014). However, the relationship between atmospheric CO_2 concentration (pCO_2) and Δ_{leaf} remains unclear and may be complicated by the drastically differing timescales (weeks to millions of years) on which Δ_{leaf} is studied. Stomata regulate leaf gas-exchange in plants to adapt to changing environments on short (weeks) and long (decades to millennia) timescales to maximize carbon (C) gain during photosynthesis and minimize water loss from transpiration (Farquhar et al., 1989; Seibt et al., 2008). Thus, shifts in Δ_{leaf} in response to short and long-term changes in pCO_2 can provide insights into the plasticity and evolution of leaf gas-exchange, which is a key goal of plant physiologists. The relationship between Δ_{leaf} and pCO_2 is also crucial for geologists because plant-derived carbon isotopes are used to infer past changes in the carbon cycle and to constrain paleoclimate and paleovegetation (e.g., Diefendorf and Freimuth, 2017).

The ratio of internal leaf CO_2 concentration (c_i) to external atmospheric CO_2 concentration (c_a), the c_i/c_a ratio, has been used as a 'set point' of leaf gas-exchange to identify how plants adapt to various environmental factors, such as pCO_2 (Ehleringer and Cerling, 1995). This ratio was also used by Farquhar et al. (1989) to model the relationship between leaf gas-exchange and carbon isotope discrimination against ^{13}C during photosynthesis (Δ_{leaf}) Eq. (1):

$$\Delta_{leaf} = a + (b - a)c_i/c_a \quad (1)$$

where a is kinetic fractionation during diffusion of air into the stomata (4.4‰) and b is the enzymatic fractionation that occurs during carboxylation due to the enzyme Rubisco strongly discriminating against ^{13}C (27‰). Δ_{leaf} can also be measured independently of the Farquhar equation using the isotopic composition of the atmosphere and a plant leaf in Eq (2):

$$\Delta_{leaf} = (\delta^{13}C_{atm} - \delta^{13}C_{leaf})/(1 + \delta^{13}C_{leaf}) \quad (2)$$

where $\delta^{13}C_{atm}$ is the carbon isotopic composition of the atmosphere and $\delta^{13}C_{leaf}$ is the carbon isotopic measurement of the leaf, both measured in ‰ relative to the standard VPDB. This equation accounts for changes in $\delta^{13}C_{atm}$ through time and, when coupled with Eq.1 and its derivatives, has been used to estimate long-term trends in c_i/c_a ratios and the intrinsic water use efficiency (iWUE) of leaf gas-exchange (Farquhar and Richards, 1984; Beerling and Woodward, 1995; Voelker et al., 2016). Therefore, Δ_{leaf} has become an important metric for understanding the relationship between c_i and c_a and for investigating how leaf gas-exchange has adapted to various environmental factors, such as pCO_2, on timescales from decades to millions of years.

Δ_{leaf} has been proposed as a proxy for reconstructing pCO_2 in the geologic record (Schubert and Jahren, 2012) based on a short-term (weeks) growth chamber study evaluating the relationship between Δ_{leaf} and pCO_2. In their growth chamber study, Schubert and Jahren (2012) observed a hyperbolic positive relationship between Δ_{leaf} and pCO_2 from 370 to 4200 ppmV using herbaceous plants, *Raphanus sativus* and *Arabidopsis thaliana*, over the course of four weeks. However, short-term growth chamber studies are prone to highly variable results. Beerling and Woodward (1995) observed no response between Δ_{leaf} and pCO_2 in their growth chamber experiment using a variety of C_3 grasses and herbs grown at 350, 525, and 700 ppmV over five weeks. Jahren et al. (2008) also observed no relationship between Δ_{leaf} and pCO_2 using *Raphanus sativus* grown over 5 weeks at 349, 389, 778, and 1088 ppmV. Conversely, Zhang et al. (2019) found a negative relationship between Δ_{leaf} and pCO_2 using *Triticum aestivum* grown between 170 and 400 ppmV. Porter et al. (2017) designed a growth chamber experiment to target Δ_{leaf} response to pCO_2 among different plant groups. The study was conducted over six-month intervals with pCO_2 at 400 and 1900 ppmV and O_2 at ambient (20.9%) and subambient (16%) levels. Two species were represented from lycophytes, monilophytes, gymnosperms, and both woody and herbaceous angiosperms. Porter et al. (2017) found Δ_{leaf} increased at the higher pCO_2 level, but the magnitude of the relationship varied among species, particularly between spore- and seed-reproducing plants. Lomax et al. (2019) grew *Arabidopsis thaliana* across a range from 380 to 3000 ppmV and found a positive, but poorly constrained relationship between Δ_{leaf} and pCO_2 that was highly variable as a function of water availability. These conflicting results among growth chamber experiments could reflect species-specific responses of stomata to pCO_2 and/or sensitivity of Δ_{leaf} to growth chamber conditions (i.e., water availability, humidity, light, nutrient-limitation, duration, and $\delta^{13}C_{atm}$). Conflicting results may also be due to growth chamber effects, caused by chamber instability or other unresolved factors (Porter et al., 2015).

Short-term (months to years) free-air CO_2 enrichment (FACE) experiments have also found variable responses of Δ_{leaf} to increased pCO_2, such as no effect (Ainsworth and Long, 2005) or a negative correlation (Battipaglia et al., 2013). Generally, FACE experiments propose plants

respond to elevated pCO_2 via changes in primary productivity, leaf gas-exchange, and stomatal attributes, but are also sensitive to nitrogen and water availability, the duration of exposure to elevated CO_2, and plant functional type (Nowak et al., 2004; Leakey et al., 2009; Mueller et al., 2016; Yan et al., 2017).

Because growth chamber studies and other short-term field studies cannot fully simulate evolutionary behavior (i.e., leaf phenotype transformations that occur across many generations) of plants in response to fluctuating pCO_2 values, the nature of this relationship has also been studied at longer timescales. For example, studies spanning decades have also found varied relationships between pCO_2 and Δ_{leaf}, but results are generally more conservative than growth chamber studies. Frank et al. (2015) measured tree ring carbon isotopes across European forests from 1901 to 2010 AD, where pCO_2 increased from 296 to 389 ppmV. After accounting for environmental effects, they found that both angiosperms and conifers were adjusting leaf gas-exchange properties to maintain a relatively constant c_i/c_a value, which is directly proportional to Δ_{leaf} based on Eq (1). A separate tree ring carbon isotope study from North America's oldest boreal trees show that Δ_{leaf} decreased between 1850 and 1965 AD as pCO_2 increased from 285 to 320 ppmV then remained constant between 1965 and 2014 as pCO_2 increased 320 and 398 ppmV (Giguère-Croteau et al., 2019). In a historical investigation of *Litsea calicaris* leaves collected from New Zealand between 1900 and 2012 AD, pCO_2 increased from 295 to 392 and had a negligible effect on leaf wax $\delta^{13}C$ values (Reichgelt et al., 2016).

Studies spanning millennia have also produced variable $\Delta_{leaf} - pCO_2$ relationships. Since the Last Glacial Maximum (LGM) (16,500 yr BP) Beerling and Woodward (1993) observed a decline in Δ_{leaf} with increasing pCO_2 in the species *Salix herbacea*. In a larger study, Becklin et al. (2014) investigated seven conifer species from the LGM to the present and found Δ_{leaf} either increased or remained constant with increasing pCO_2, but that leaf physiological responses to changing climate and environment differed in timing and magnitude. In a Miocene-aged study from New Zealand, sediment leaf waxes were extracted from a varved maar formation spanning 100,000 yrs in a subtropical environment (Reichgelt et al., 2016). The calculated Δ_{leaf} values represent an ecosystem signal integrated over millennia. In this study, Reichgelt et al. (2016) found that higher Δ_{leaf} values corresponded with higher pCO_2 values. However, the hydrogen isotope composition of these same leaf waxes indicate that water availability, not pCO_2, was the main driver of plant physiological change (Reichgelt et al., 2016).

On million-year timescales, only a few studies have investigated how Δ_{leaf} responds to pCO_2. Diefendorf et al. (2015a) analyzed sediment leaf wax from Paleocene and Eocene paleoflora sites in the Bighorn Basin (WY, USA) and found Δ_{leaf} values were not sensitive to changes in pCO_2. Instead, Δ_{leaf} values varied with paleoprecipitation trends, similar to the Δ_{leaf} – mean annual precipitation (MAP) relationship from modern calibrations (Diefendorf et al., 2010; Kohn, 2010). Kohn (2016) used $\delta^{13}C$ values of herbivore tooth enamel to constrain C_3 plant $\delta^{13}C$ values through the Cenozoic, ranging between 200 and 700 ppmV and found that pCO_2 had a negligible relationship with Δ_{leaf} and variations in Δ_{leaf} were likely driven by water availability.

Taking all this prior work together, there is little consensus on how high pCO_2 effects Δ_{leaf}, especially over long-time scales and at pCO_2 higher than 700 ppm. Therefore, we investigate the relationship between Δ_{leaf} and pCO_2, and the efficacy of this relationship to reconstruct pCO_2 through geologic time by utilizing the geologic record as a natural laboratory operating on timescales over which plants evolve (millions of years). In our study, we measured $\delta^{13}C$ values from sediment-derived leaf wax n-C_{29} alkanes, primarily from angiosperms, to calculate Δ_{leaf} across North American paleoflora sites. These sites represent 40 million years from the Late Cretaceous into the Oligocene and capture a wide range of pCO_2 values (200–900 pmmV; Foster et al., 2017). Hyperthermal time periods are avoided in order to avoid confounding effects of rapid climate perturbations on plants. Using the fossil leaves at each site, we account for age, floral composition, mean annual precipitation (MAP), and mean annual temperature (MAT), thereby providing a means to test the sensitivity of Δ_{leaf} to pCO_2 independent of confounding biotic and abiotic effects on geologic timescales.

2. METHODS

2.1. Site Information

Sediment samples were collected across North America from 26 leaf fossil sites (Fig. 1). These sites were all previously characterized in paleobotanical studies and represent a range of depositional environments, water regimes, temperatures, and pCO_2 concentrations (Table 1). The Δ_{leaf} values from 8 sites in the Bighorn Basin, Wyoming were previously reported in Diefendorf et al. (2015a).

Sample sites range from the High Arctic to New Mexico, spanning modern latitudes of 82–36°N and include localities from Ellesmere and Axel Heiberg islands, the Okanagan Highlands in British Columbia, the Wind River and Bighorn Basins in Wyoming, various intermontane basins in Colorado and Utah, and the San Juan Basin in New Mexico. Paleoelevations ranged from 0 to 3 km (Gregory and McIntosh, 1996; Smith et al., 2009; Zaborac-Reed and Leopold, 2016). The geographic location, age, MAP, MAT, $\delta^{13}C_{atm}$, and pCO_2 are constrained for each locality (Table 1). Ages for each locality were extracted from the literature and were determined using a variety of dating techniques (i.e., biostratigraphy, magnetostratigraphy, $^{40}Ar/^{39}Ar$ dating, U-Pb dating) (see Table 1). Geologic ages were used to constrain $\delta^{13}C_{atm}$ and pCO_2 values at each site. The $\delta^{13}C_{atm}$ values were taken from Tipple et al. (2010) for Cenozoic sites and Barral et al. (2017) for Cretaceous sites. In these studies, $\delta^{13}C_{atm}$ values were calculated from $\delta^{13}C$ and $\delta^{18}O$ records of benthic foraminifera and are corrected for temperature-sensitive equilibrium and non-equilibrium isotope effects between carbonate minerals and atmospheric CO_2 and averaged across 3-million-year windows. The pCO_2 values, taken from Foster et al.

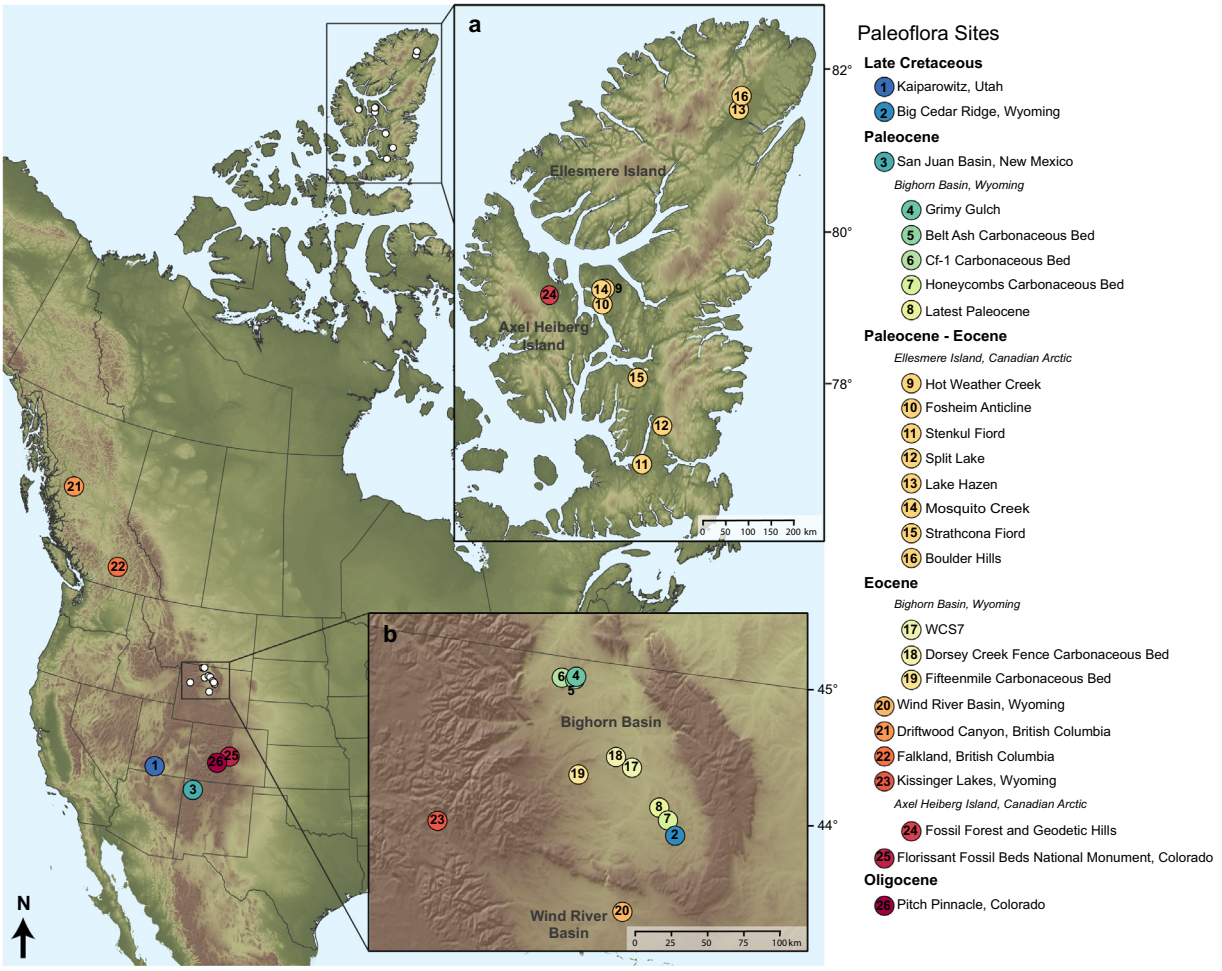

Fig. 1. Map of North America depicting paleoflora sites used in this study. Numbered circles indicate paleoflora sampling localities with a corresponding key to the right of the map. Sites are listed from oldest to youngest and colors correspond to age. Cool colors (blues) denote older sites and warmer colors (reds) denote younger sites. Panel (a) shows a close up of Ellesmere and Axel Heiberg islands. Panel (b) is an expanded map of the Bighorn and Wind River basins.

(2017), are derived from a Monte Carlo resampled time series of a compilation of pCO_2 proxies including leaf stomata, pedogenic carbonates, boron isotopes, liverworts, and alkenones. The $\delta^{13}C_{atm}$ and pCO_2 values through the study interval are shown in Fig. 2. Estimates of MAP were determined for each site using leaf area analysis (LAA) (Wilf et al., 1998). For Florissant and Pitch Pinnacle, paleoprecipitation was estimated prior to LAA and was measured using the climate leaf analysis multivariate program (CLAMP) (Wolfe, 1993). However, LAA was recently performed on the paleoflora of Florissant (Allen et al., 2017) and falls within ±25 cm of the previous CLAMP estimate, and is consistent with a MAP < 100 cm/yr. Estimates of MAT were obtained from previous paleobotanical studies and were determined using the nearest living relative (NLR) method, leaf margin analysis (LMA) (Wing and Greenwood, 1993; Miller et al., 2006), or CLAMP (see Supplementary Data 2).

Sediment samples were collected from fossil leaf-bearing zones and consist of sandstones, siltstones, shales, mudstones, lignites, and coals and represent an integrated signal of many species and individuals. We targeted zones of low pedogenesis and wet fluvial, lacustrine, swamp, and floodplain depositional environments to reduce effects of water stress. Between 1 and 20 sediment samples with minimal weathering were collected laterally across fossil-bearing zones at each paleoflora site. Sediments were then oven dried (60 °C) and between 15 and 30 g of sediment were powdered using a ball mill and split into two fractions, one for lipid extraction and one for bulk carbon isotopes ($\delta^{13}C_{bulk}$).

2.2. Lipid extraction from sediments

To target n-C_{29} alkanes for analysis, lipids were extracted from powdered samples using an accelerated solvent extractor (Dionex ASE 350) with 5:1 (v/v) DCM/MeOH. From the total lipid extract (TLE), asphaltenes were precipitated with DCM/Hexanes (1:80 v/v). The maltene fraction was extracted from the hexanes and further

Table 1
Site info and climate data for each paleoflora locality.

Site #	Site name	Location	Age (Ma)	pCO_2 (ppmV) ± 95%CI[q]	$\delta^{13}C_{atm}$ (‰) ± 90%CI[r,s]	MAP (cm/yr), ±1SE	MAT (°C) ± 1SE
	Late Cretaceous						
1	Kaiparowits	UT, USA	75.05 ± 1.05[a]	552 + 421/−320	−6.5 ± 0.75	178 + 77/−54[a]	20.16 ± 2.33[a]
2	Big Cedar Ridge	Bighorn Basin, WY, USA	72.7 ± 1.43[b]	417 + 352/−255	−6.5 ± 0.75	wet[u]	20[b]
	Paleocene						
3	SJB Pu2 site	San Juan Basin, NM, USA	65.55 ± 0.05[c]	234 + 186/−89	−4.5 ± 0.75	197.4 + 89.5/−62.5[v]	20.2 ± 2.93[v]
4	Grimy Gulch	Bighorn Basin, WY, USA	63 ± 1.5[d]	287 + 161/−86	−5.5 ± 0.75	120*[d]	n.d.
5	Belt Ash	Bighorn Basin, WY, USA	59.39 ± 1.5[d]	373 + 158/−102	−4.8 ± 0.75	120 + 52/−36[d]	10.5 ± 2.9[d]
6	Cf-1	Bighorn Basin, WY, USA	57.39 ± 1.5[d]	477 + 140/−123	−4.4 ± 0.75	109 + 47/−33[d]	12.0 ± 2.9[d]
7	Honeycombs	Bighorn Basin, WY, USA	56.1 ± 1.5[d]	539 + 139/−137	−4.6 ± 0.75	173*[d]	16.4 ± 2.9[d]
8	Latest Paleocene	Bighorn Basin, WY, USA	56.04 ± 1.5[d]	539 + 139/−137	−4.7 ± 0.75	173 + 75/−52[d]	16.4 ± 2.9[d]
	Paleocene - Eocene						
9	Hot Weather Creek	Ellesmere Island, Canada	57.6 ± 1.6[e]	463 + 142/−121	−4.4 ± 0.75	143 + 63/−43[e]	13.5 ± 1.5[i]
10	Fosheim Anticline	Ellesmere Island, Canada	57.6 ± 1.6[e]	463 + 142/−121	−4.4 ± 0.75	153 + 66/−46[e]	13.5 ± 1.5[i]
11	Stenkul Fiord	Ellesmere Island, Canada	57–53.1[f,g,h]	599 + 145/−148	−4.9 ± 0.75	240 + 104/−72[t]	8.5 ± 2.6[t]
12	Split Lake	Ellesmere Island, Canada	53.9 ± 3.1[g,i]	463 + 142/−121	−4.4 ± 0.75	228 + 98/−69[t]	12.4 ± 3.8[t]
13	Lake Hazen	Ellesmere Island, Canada	51.9 ± 4.1[j]	660 + 238/−181	−5.0 ± 0.75	143 + 63/−43[e]	13.5 ± 1.5[i]
14	Mosquito Creek	Ellesmere Island, Canada	53.5 ± 5.7[j]	660 + 213/−164	−5.0 ± 0.75	143 + 63/−43[e]	13.5 ± 1.5[i]
15	Strathcona Fiord	Ellesmere Island, Canada	51.9 ± 4.1[i,j]	735 + 238/−181	−5.4 ± 0.75	230 + 99/−69[t]	12.4 ± 3.8[t]
16	Boulder Hills	Ellesmere Island, Canada	42.9 ± 4.9[j]	777 + 236/−196	−5.9 ± 0.75	133 + 57/−40[e]	12.8 ± 4.3[e]
	Eocene						
17	WCS7	Bighorn Basin, WY, USA	55.34 ± 1.5[d]	598 + 145/−147	−4.9 ± 0.75	173 + 75/−52[d]	16.4 ± 2.7[d]
18	Dorsey Creek Fence	Bighorn Basin, WY, USA	54.37 ± 1.5[d]	653 + 158/−156	−5.2 ± 0.75	132 + 57/−40[d]	10.8 ± 3.3[d]
19	Fifteenmile Creek	Bighorn Basin, WY, USA	52.98 ± 1.5[d]	721 + 206/−168	−5.6 ± 0.75	114 + 49/−34[d]	22.2 ± 2.0[d]
20	Wind River Basin	Wind River Basin, WY, USA	52.42 ± 0.06[k]	744 + 226/−173	−5.9 ± 0.75	154 + 66/−46[k]	20.4 ± 2.4[k]
21	Driftwood Canyon	British Columbia, Canada	51.77 ± 0.34[l]	743 + 267/−160	−6.0 ± 0.75	116 + 50/−35[w]	6.8 ± 2.0[w]
22	Falkland	British Columbia, Canada	50.61 ± 0.16[m]	813 + 297/−206	−5.7 ± 0.75	121 + 52/−37[m]	10 ± 2.2[m]
23	Kissinger Lakes	Wind River Basin WY, USA	49.12 ± 0.88[k]	844 + 327/−230	−5.5 ± 0.75	119 + 51/−36[k]	14.6 ± 3.0[k]
24	Fossil Forest and Geodetic Hills	Axel Heiberg Island, Canada	44.5 ± 3.3[i]	762 + 257/−204	−5.9 ± 0.75	133 + 57/−40[e]	12.8 ± 4.3[e]
25	Florissant	Florissant Fossil Beds National Monument, CO, USA	34.07 ± 0.1[o]	897 + 98/−177	−6.0 ± 0.75	64.7 ± 18.9[x]	10.7 ± 1.5[x]
	Oligocene						
26	Pitch Pinnacle	CO, USA	30.95 ± 1.95[p]	752 + 83/−118	−6.2 ± 0.75	136[y]	12.7 ± 1.5[p]

[a] Miller et al., 2013; [b] Wing and Greenwood, 1993; [c] Mason, 2013; [d] Diefendorf et al., 2015a; [e] Greenwood et al., 2010; [f] Harrison et al., 1999; [g] Reinhardt et al., 2013; [h] Reinhardt et al., 2017; [i] Eberle and Greenwood, 2012; [j] McIver and Basinger, 1999; [k] Currano et al., 2019; [l] Moss et al., 2005; [m] Smith et al., 2012; [o] Evanoff et al., 2001; [p] Gregory and McIntosh, 1996; [q] Foster et al., 2017; [r] Tipple et al., 2010; [s] Barral et al., 2017; [t] West et al., 2015; [u] Wing et al., 2012; [v] Geng et al., 2018; [w] Greenwood et al., 2005; [x] Gregory and McIntosh, 1996; [y] Barton, 2006; *Estimated, see Diefendorf et al., 2015a.

divided into apolar and polar fractions on alumina oxide with hexanes/DCM (9:1 v/v) and DCM/MeOH (1:1 v/v), respectively. The apolar fraction was then separated into saturated and unsaturated fractions on 5% Ag-impregnated silica gel (w/w) with hexanes and ethyl acetate, respectively.

2.3. Compound identification and quantification

To identify and quantify *n*-alkanes, aliquots of the apolar saturated fraction were dissolved in hexane and injected into an Agilent 7890A gas chromatograph (GC) interfaced to an Agilent 5975C quadrupole mass selective detector (MSD, operated at 70 eV) and flame ionization detector (FID). Compounds were separated on a fused silica capillary column (Agilent J&W DB-5 ms; 30 m length, 0.25 mm i.d., 0.25 μm film thickness). The oven program ramped from an initial temperature of 60 °C for 1 min, followed by a 6 °C/min temperature ramp to 320 °C and held for 15 min. Following the GC separation, the column effluent was split (1:1) between the FID and MSD with a 2-way splitter, using He makeup gas to keep pressure constant. Compounds were identified using authentic standards, fragmentation patterns, and retention times.

Quantification by FID was achieved by normalizing compound peak areas to an internal standard (1,1′-binaphthalene) and converting normalized peak areas to mass using external standard response curves (also normalized to the internal standard). The external standard curves ranged in concentration from 0.5 to 100 μg/ml and included a series of *n*-alkanes of varying chain length, from C_7 to C_{40} (Sigma Aldrich). Finally, compound concentrations were normalized to the dry sediment mass (μg/g).

2.4. Bulk Carbon Analysis

To remove carbonate minerals, samples were exposed to 1 N HCl for 30 minutes or until reaction was complete and neutralized using DI water rinses before bulk isotope analysis. The $\delta^{13}C$ of bulk organic carbon and weight percent of total organic carbon (wt.% TOC) were determined via continuous flow (He; 120 ml/min) on a Costech elemental analyzer (EA) coupled to a Thermo Electron Delta V Advantage Isotope Ratio Mass Spectrometer (IRMS). $\delta^{13}C$ values were corrected for sample size dependency and normalized to the VPDB scale using a two-point calibration (e.g., Coplen et al., 2006). Error was determined by analyzing additional independent standards measured in all EA runs. Long term combined precision and accuracy of all EA runs was 0.12‰ (1σ; n = 30) and −0.13‰ (n = 30), respectively.

2.5. Compound-specific carbon isotope analysis

Compound-specific carbon isotope analyses of the *n*-alkanes were performed by GC–combustion (C)–IRMS. Based on whether *n*-C_{29} or *n*-C_{31} alkanes were eluting with other compounds, some samples were first separated into branched and *n*-alkyl fractions using urea adduction. GC–C-IRMS was performed using a Thermo Trace GC Ultra coupled to an Isolink combustion reactor (Ni, Cu, and Pt wires) and Thermo Electron Delta V Advantage IRMS. Isotopic abundances were normalized to the VPDB scale using Mix A6 (Arndt Schimmelmann, Indiana University). Carbon isotope precision (0.41‰; 1σ) and accuracy (0.11‰; 1σ) were monitored across all standard and sample runs with co-injected *n*-C_{41} alkane (n = 317). Additionally, an in-house *n*-alkane standard prepared from oak leaves (Oak-1a) was analyzed every 5–6 runs with a precision and accuracy for *n*-C_{29} of 0.18‰ (1σ; n = 30) and 0.02‰ (n = 30) and for *n*-C_{31} of 0.24‰ (1σ; n = 30) and −0.08‰ (n = 30), respectively.

2.6. Calculating Δ_{leaf}

To minimize potential effects of vegetation composition on Δ_{leaf} (e.g., due to differences in the relative abundance of angiosperms and gymnosperms), the $\delta^{13}C$ values of *n*-C_{29} and *n*-C_{31} alkanes were used to calculate Δ_{leaf}. Previous studies suggest these long chain *n*-alkanes are primarily derived from woody angiosperms (Diefendorf et al., 2011; Bush and McInerney, 2013). Therefore, the *n*-alkanes preserved in the sediment should represent C_3 woody angiosperm vegetation across our range of paleoflora sites. The $\delta^{13}C$ values of *n*-alkanes were first converted to $\delta^{13}C_{leaf}$ values to account for biosynthetic fractionation ($\varepsilon_{n\text{-}C29\ -\ leaf}$) that occurs during the synthesis of *n*-alkanes:

$$\varepsilon_{n-C29-leaf} = (\delta^{13}C_{n-C29} + 1)/(\delta^{13}C_{leaf} + 1) \quad (3)$$

where the *n*-C_{29} alkane homologue is shown as an example. The $\varepsilon_{n\text{-}C29\text{-}leaf}$ and $\varepsilon_{n\text{-}C31\text{-}leaf}$ values used in this study were derived from a global compilation of woody vegetation (Diefendorf and Freimuth, 2017) and were 5.2‰ and 5.6‰, respectively. Δ_{leaf} was then calculated using $\delta^{13}C_{leaf}$ values and Eq. (2). Average Δ_{leaf} values from both *n*-C29 and *n*-C31 alkanes for each paleoflora location are reported in Table 2. The Δ_{leaf} measures the difference between the carbon isotopic composition of the atmosphere and the leaf, thus accounting for changes in $\delta^{13}C_{atm}$ through time.

2.7. Quantifying uncertainty in Δ_{leaf} and additional statistical analyses

A Monte Carlo simulation method was performed to quantify Gaussian uncertainty (1σ) in Δ_{leaf} values for each site using 10,000 iterations in MATLAB R2017a (The MathWorks, Natick, USA). Input uncertainties included $\delta^{13}C_{atm}$, intrasite variability of $\delta^{13}C_{n\text{-}C29}$ values, and $\varepsilon_{n\text{-}C29}$. The $\delta^{13}C_{atm}$ values were obtained using a 3-million-year window and uncertainties (0.75‰) represent the high and low 90% confidence intervals reported in Tipple et al. (2010). For $\delta^{13}C_{n\text{-}C29}$ values, uncertainty was determined using the one standard deviation of intrasite variability at each site. These values ranged from 0.5‰ to 1.35‰. Uncertainty in $\varepsilon_{n\text{-}C29}$ (2.4‰) and $\varepsilon_{n\text{-}C31}$ (2.5‰) was determined from the one standard deviation in a global compilation of angiosperm $\varepsilon_{n\text{-}C29}$ values reported in Diefendorf and Freimuth (2017). Most of the total uncertainty in our Δ_{leaf} values is driven by uncertainty in the ε values. Several studies have argued that modern calibrations have much higher

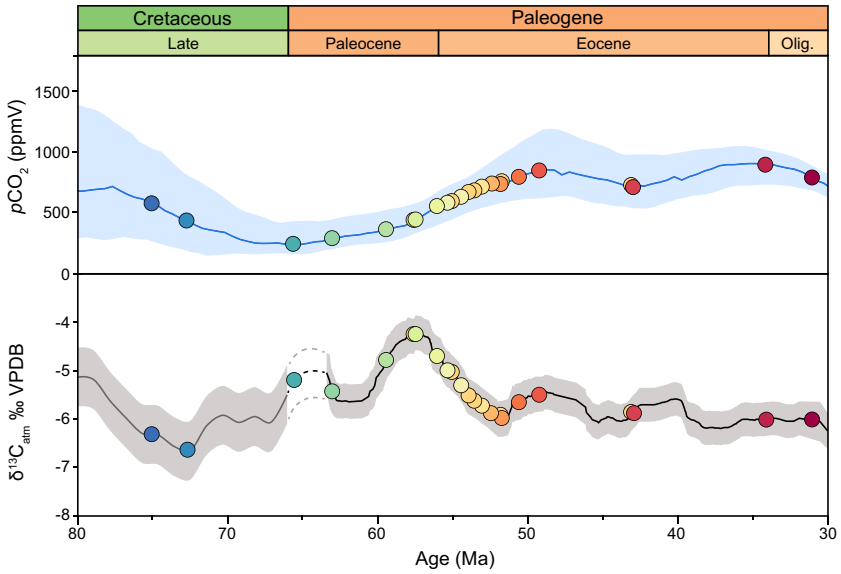

Fig. 2. Atmospheric pCO_2 concentrations (top) and the $\delta^{13}C$ of atmospheric CO_2 (bottom) plotted from the Late Cretaceous to the Oligocene. Circles represent ages where samples were collected. See Fig. 1 for colors and corresponding site information. Atmospheric pCO_2 concentrations are from Foster et al. (2017) and were determined from multiple pCO_2 proxies. The blue line indicates mean values with 95% confidence intervals shown in light blue. The $\delta^{13}C$ of atmospheric CO_2 is based on the $\delta^{13}C$ of benthic foraminifera and redrawn from Barral et al., 2017 (grey line, 1×10^6 yr running average) and Tipple et al., 2010 (black line, 3×10^6 yr running average). The gray shaded regions represent their reported 90% confidence intervals. Dashed line represents data not included in the running averages. For the sample collected during this interval, we use the 0.5×10^6 yr running average reported in Tipple et al. (2010).

ranges of variability in ε values than would be expected from geologic sediment, which represents many integrated plants through time (Polissar et al., 2009; Diefendorf and Freimuth, 2017). Therefore, the total uncertainty represented in our Δ_{leaf} values is likely an overestimate.

Simple and multiple linear regression analyses were used to assess the relationships between various predictors (e.g., pCO_2 and MAP) and Δ_{leaf}. These and other simple statistical analyses, including Student's t-tests, were carried out using JMP Pro 14.0 (SAS, Cary, USA), using site-averaged Δ_{leaf} values.

3. RESULTS

3.1. Leaf carbon isotope fractionation data

The Δ_{leaf} values calculated from either *n*-C29 or *n*-C31 alkanes were similar for all sites (t-test, $p = 0.995$) (Table 2). Further discussion of Δ_{leaf} values focus on results from *n*-C_{29} alkanes. Intra-site variability of Δ_{leaf} values were less than 2.8‰ at all but one paleoflora site. Sites with larger ranges in Δ_{leaf}, such as Stenkul Fiord (4.2‰), contain a mix of different lithologies (coals and siltstones). These different depositional environments likely represents a more diverse spectrum of water regimes and vegetation composition. The sediment Δ_{leaf} values encompass many species and individuals, resulting in a more conservative range than the 8‰ range observed among modern forest sites with high species diversity (e.g., Diefendorf et al., 2010).

Site-averaged Δ_{leaf} values vary from 17.7 to 22.6‰, showing a 4.9‰ range over 40 million years, spanning diverse climates, environments, and vegetation across the paleoflora sites (e.g., ≥175 cm/yr range in MAP and ≥15 °C range in MAT). We do observe some trends in Δ_{leaf} through time (Fig. 3). Δ_{leaf} values increase steadily from 20.1‰ during the Late Cretaceous at Kaiparowits to 21.5‰ in the early Paleocene at SJB Pu2 site and reach 22.6‰ during the late Paleocene at Honeycombs Carbonaceous Bed. Δ_{leaf} values begin to decrease during the Early Eocene and continue to decrease throughout the middle Eocene. Δ_{leaf} values reach a low of 17.7‰ in the present study during the Oligocene at Pitch Pinnacle.

3.2. Δ_{leaf} relationships to pCO_2 and climate

Over a 700 ppmV increase in pCO_2, Δ_{leaf} decreases by 3.4‰ (Fig. 4). However, variables other than pCO_2 may also be affecting Δ_{leaf}. Therefore, a series of simple linear regressions were performed to explore the sensitivity of Δ_{leaf} to various climate, environmental, and preservational factors including pCO_2, Log_{10}MAP, MAT, latitude, average chain length (ACL), carbon preference index (CPI), and total organic carbon (TOC) (Supplementary Data 1; Table 1). MAP was log transformed because it is logarithmically related to Δ_{leaf} and thereby satisfies normality requirements (Diefendorf et al., 2010). Differences in methodology used to calculate MAT from leaf fossils may lead to significant variances in temperature estimates, though estimates from different methods are often close to or within uncertainty (Peppe et al., 2018). However, when evaluating the relationship between Δ_{leaf} and MAT, we find no relationship ($p = 0.34$), making it unlikely that

Table 2
Calculated Δ_{leaf} values using both n-C_{29} and n-C_{31} alkanes for each paleoflora site.

Site #	Site name	$\Delta_{leaf\ (n\text{-}C29)}$	1σ	n	$\Delta_{leaf\ (n\text{-}C31)}$	1σ	n
	Late Cretaceous						
1	Kaiparowits	20.1	2.6	20	20.4	2.8	20
2	Big Cedar Ridge[a]	20.6	2.6	36	20.3	2.7	36
	Paleocene						
3	SJB Pu2 site	21.5	2.6	13	21.9	2.8	13
4	Grimy Gulch[b]	21.7	2.8	7	21.8	3.0	7
5	Belt Ash Carbonaceous Bed[b]	20.9	2.8	4	21.2	2.7	4
6	Cf-1 Carbonaceous Bed[b]	21.9	2.7	4	21.6	2.8	4
7	Honeycombs Carbonaceous Bed[b]	22.6	2.7	5	22.4	2.9	5
8	Latest Paleocene[b]	21.6	2.7	5	21.5	2.8	5
	Paleocene - Eocene						
9	Hot Weather Creek	20.7	2.9	3	21.7	2.7	2
10	Fosheim Anticline	21.8	n.d.	1	21.7	n.d.	1
11	Stenkul Fiord	21.7	2.8	18	20.6	2.8	17
12	Split Lake	20.6	n.d.	1	20.6	n.d.	1
13	Lake Hazen	19.1	n.d.	1	20.5	n.d.	1
14	Mosquito Creek	20.0	n.d.	1	19.2	n.d.	1
15	Strathcona Fiord	19.7	n.d.	1	20.4	n.d.	1
16	Boulder Hills	19.9	n.d.	1	20.0	n.d.	1
	Eocene						
17	WCS7[b]	21.6	2.6	4	21.7	2.7	4
18	Dorsey Creek Fence Carb. Bed[b]	20.7	2.6	3	21.2	2.7	2
19	Fifteenmile Carbonaceous Bed[b]	21.4	2.6	10	21.4	2.8	10
20	Wind River Basin	19.8	2.7	20	20.6	2.7	14
21	Driftwood Canyon	20.5	2.7	13	20.6	2.7	8
22	Falkland	20.0	n.d.	1	19.9	n.d.	1
23	Kissinger Lakes	20.5	2.7	6	21.4	2.8	6
24	Fossil Forest and Geodetic Hills	19.2	2.6	2	19.0	2.7	1
25	Florissant	18.1	2.6	14	18.3	2.7	13
	Oligocene						
26	Pitch Pinnacle	17.7	2.6	6	17.1	2.7	6
	Cross-site Average	20.5	2.7	27	20.7	2.8	27

[a] Bush, 2014;
[b] Diefendorf et al., 2015a,b.

use of different MAT calibrations would significantly affect the results. The simple linear regressions indicate that pCO_2 and MAP had the greatest explanatory power on Δ_{leaf} values ($p < 0.0001$; $R^2 = 0.35$; 0.33, respectively).

To assess the effects of pCO_2 on Δ_{leaf} independently of MAP and vice versa, a multiple linear regression analysis was performed using Δ_{leaf} as the dependent variable and pCO_2 and Log_{10}MAP as independent variables (Supplementary Date 1; Table 2). The predicted Δ_{leaf} is equal to 14.03091125–0.00318293 (pCO_2) + 2.6765392395 (Log_{10}-MAP) (R^2 of 0.49, ($F[2, 161] = 77.7834$, $p < 0.0001$). Both pCO_2 and Log_{10}MAP were significant predictors of Δ_{leaf} ($p < 0.0001$) with opposite influences. The negative correlation between Δ_{leaf} and pCO_2 is consistent with the findings of Kohn (2016) and the significance of water availability is consistent with Lomax et al. (2019), whose growth chamber study directly tested the role of water availability on the $\Delta_{leaf} - pCO_2$ relationship. Based on the multiple regression model, if mean pCO_2 were to increase by 25% (~150 ppmV) while mean MAP is held constant, Δ_{leaf} should decrease by 0.46‰. At wetter sites (>1500 mm/yr), if mean MAP were to increase by 25% (~400 mm/yr) while pCO_2 were held constant, Δ_{leaf} should increase by 0.26‰. Because MAP is a log function, if ~400 mm/yr were added to the driest range of MAP while pCO_2 were held constant, Δ_{leaf} should increase by 0.54‰. After accounting for variations in MAP, Δ_{leaf} is still sensitive to pCO_2 (-0.3 ± 0.09‰/100 ppmV) between 200 and 900 ppmV. This is consistent with low Δ_{leaf} values at Florissant and Pitch Pinnacle when reconstructed pCO_2 values were highest (897 and 752 ppmV, respectively; Fig. 4; Foster et al., 2017).

Additional multiple linear regression analyses were performed to assess the explanatory power of pCO_2 and MAP when other variables (i.e., MAT and age) are included (Supplementary Data 1; Table 3). We find that the statistical significance of pCO_2 and MAP persist. Temporal variability has little apparent effect on Δ_{leaf} when pCO_2, MAP, MAT, and age are included in the model. We also found no apparent effect of temporal variability on Δ_{leaf} when MAT is excluded while pCO_2, MAP, and age are

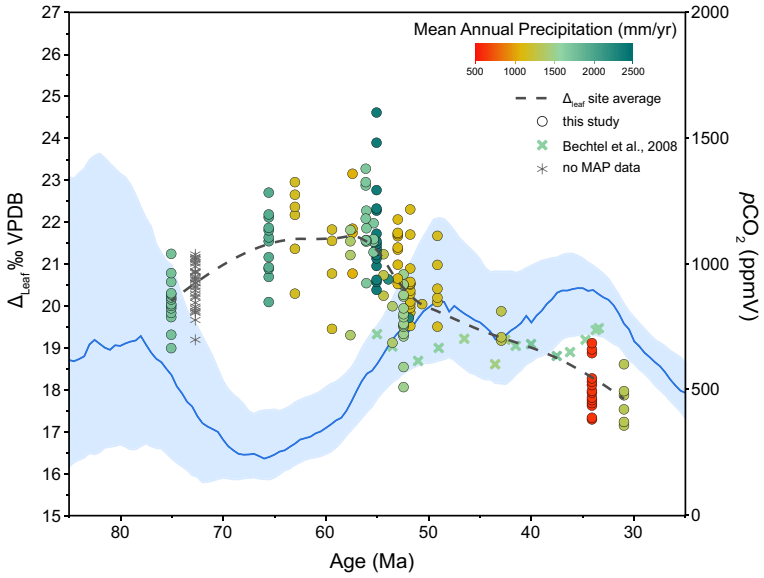

Fig. 3. Δ_{leaf} values from all paleoflora sites and samples. Each dot represents an individual sample (plant waxes extracted from a bulk rock sample) collected laterally across a leaf bearing zone at the same site. Points are colored by mean annual precipitation, measured from the leaf fossil data, and are reported in Table 1. The dashed gray line represents site-averaged Δ_{leaf} values. pCO_2 values (blue line) are from Foster et al. (2017) and the shaded blue region represents their reported 95% confidence interval.

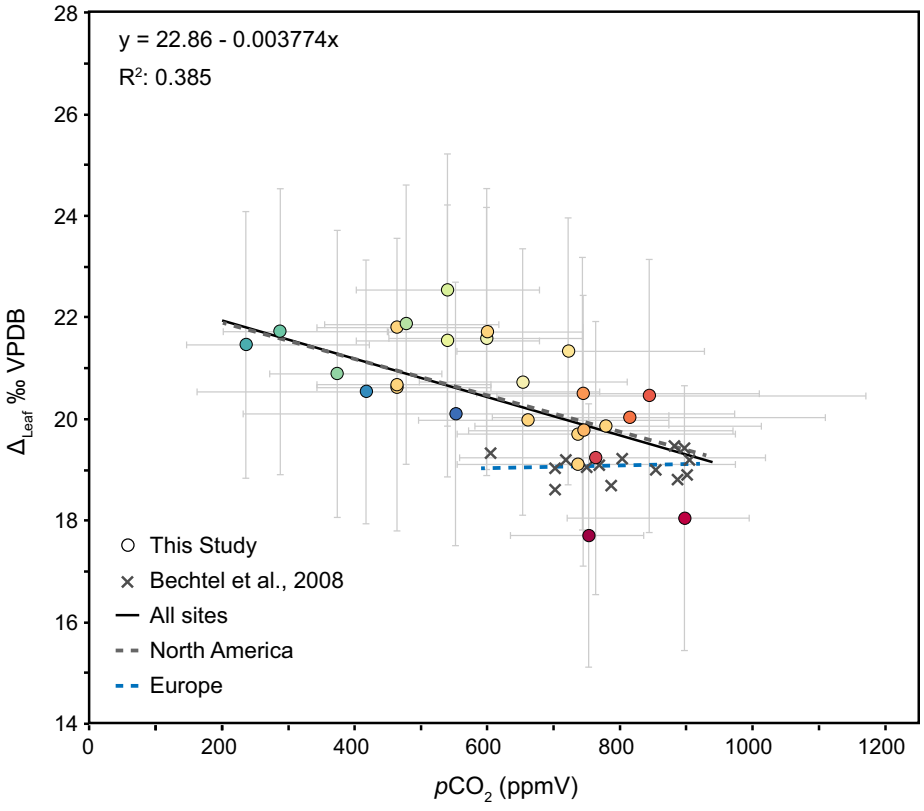

Fig. 4. Site-averaged Δ_{leaf} values for each sampling site reported against independent proxy-based pCO_2 estimates (Foster et al., 2017). Site information is color coded and corresponds to those reported in Fig. 1. Error bars for Δ_{leaf} in the y-axis represent combined uncertainty calculated using a Monte Carlo method and takes into account uncertainties in the $\delta^{13}C_{n\text{-}C29}$, $\varepsilon_{n\text{-}C29\ -\ leaf}$, and $\delta^{13}C_{atm}$ values. Error bars for pCO_2 in the x-axis represent the upper and lower 95% confidence intervals determined by Foster et al. (2017) for each sample age range. Additional samples from Bechtel et al. (2008) are also included for comparison and were derived from low-rank coal deposits from the Alpine Realm and Middle German Lignite District from the Eocene and Oligocene. The linear regression analysis equation includes all data shown.

Table 3
Conifer abundances, their relative *n*-C_{29}-alkane production, and paleobotanical references for each general location.

Site location	Conifer abundance[†]	Conifers (*n*-C_{29}-alkane production)	Paleobotanical reference
Kaiparowits	Rare	Cupressaceae sp. (low)	Miller et al., 2013
Big Cedar Ridge	Rare	Cupressaceae sp. (low), *Araucarites* sp, (moderate)	Wing et al., 2012
San Juan Basin	Rare	*Cupressinocladus* (low), *Ditaxocladus* (low)	Flynn et al., in press
Bighorn Basin Sites	Common	*Metasequoia* (low), *Glyptostrobus* (low)	Davies-Vollum and Wing, 1998; Smith et al., 2007; Diefendorf et al., 2014; Diefendorf et al., 2015a
Ellesmere Isl Sites	Common	*Metasequoia* (low), *Glyptostrobus* (low), *Chamaecyparis* (low)	Eberle and Greenwood, 2012; West et al., 2015; West et al., 2019
Wind River Basin	Absent	–	Currano et al., 2019
Driftwood Canyon	Common	*Metasequoia* (low), *Sequoia* (low), *Chamaecyparis* (low), *Thuja* (low), Pinaceae (low)	Eberle et al., 2014
Falkland	Common	*Metasequoia* (low), *Glyptostrobus* (low), *Taxodium* (low), *Sequoia* (low), *Chamaecyparis* (low), Pinaceae (low)	Smith et al., 2012
Kissinger Lakes	Present*	–	Leopold, 1974; Currano et al., 2019
Axel Heiberg Isl Sites	Common	*Metasequoia* (low), *Glyptostrobus* (low), *Chamaecyparis* (low), Pinaceae (low)	McIver and Basinger, 1999; Eberle and Greenwood, 2012
Florissant	Common	*Sequoia* (low), *Chamaecyparis* (low), *Torreya* (low), *Abies* (low), *Picea* (low), *Pinus* (low)	Gregory, 1994; Manchester, 2001
Pitch Pinnacle	Uncommon	*Juniperus* (low), *Abies* (low), *Picea* (low), *Pinus* (low)	Gregory and McIntosh, 1996

[†] Approximated from biomass.
* Based on pollen data, no conifers present in macroflora.

included. Accounting for temporal variability helps rule out alternative explanations, such temporal shifts in plant physiology or other unmeasured temporal variability, that might misconstrue the correlations observed between Δ_{leaf} and pCO_2 and MAP through geologic time.

3.3. Additional Δ_{leaf} records

To increase the scope of this study beyond North America, an additional subset of low rank coal $\delta^{13}C$ data was included from Bechtel et al. (2008) that overlap with the ages of our study and encompass the Alpine Realm and Middle German Lignite District of Europe. This subset spans the Early Eocene into the Oligocene (55–33.4 Ma, 600–900 ppmV for pCO_2). The reported $\delta^{13}C$ values were corrected for liptinite, hopanoids, and angiosperm vs. gymnosperm input (Bechtel et al., 2008) and represent a mix of plant matter from resin, leaves, spores/pollen, and bark. We converted the $\delta^{13}C$ values to Δ_{leaf} values as previously described (see Section 2.6). The resulting Δ_{leaf} values span a smaller range (18.6–19.5‰) than our North American study (Fig. 3). One possible explanation might be because these samples were all deposited in similar swampy depositional environments with MAP > 1500 mm/yr (Bechtel et al., 2008). Linear regression analysis of the Bechtel et al. (2008) data indicates no correlation between Δ_{leaf} and pCO_2 ($p = 0.74$, n = 14; Fig. 4). However, when the Bechtel data was included with our North American data, linear regression indicates that Δ_{leaf} is still significantly correlated with pCO_2 ($R^2 = 0.39$, $p < 0.0001$, n = 214) and corresponds to -0.37 ± 0.08‰/100 ppmV between 200 and 900 ppmV.

4. DISCUSSION

4.1. Δ_{leaf} as a paleo-pCO_2 proxy

Δ_{leaf} is regularly used in paleoclimate and paleovegetation applications because of its sensitivity to environmental and ecological factors, including water availability (Diefendorf et al., 2010; Kohn, 2010) and photosynthetic pathway (i.e., C_3 vs. C_4 photosynthesis). However, the effects of pCO_2 on Δ_{leaf} and its use as a proxy for pCO_2 over geologic time has remained unclear and controversial (e.g., Schubert and Jahren, 2012; Diefendorf et al., 2015a; Cui and Schubert, 2016; Kohn, 2016; Lomax et al., 2019; Porter et al., 2019; Zhang et al., 2019). By converting sediment *n*-alkane $\delta^{13}C$ values to Δ_{leaf} and using modern calibrations and other proxy data to constrain effects of vegetation and precipitation, we assessed the sensitivity of Δ_{leaf} to pCO_2 as it varied from 200 to 900 ppmV among paleoflora sites in North America. We found that Δ_{leaf} has a small negative response to increasing pCO_2 (-0.3 ± 0.09‰/100 ppmV) from the Late Cretaceous through the Paleogene, when accounting for precipitation. This study shows pCO_2 has a somewhat more negative effect

on Δ_{leaf} values than previous geologic studies that found no relationship (Diefendorf et al., 2015a) or a small negative relationship (-0.03 ± 0.24‰/100 ppmV between 370 and 715 ppmV) (Kohn, 2016).

Based on the short-term growth chamber study by Schubert and Jahren (2012), some studies use Δ_{leaf} as a paleo pCO_2 proxy in the geologic record (Schubert and Jahren, 2012; Cui and Schubert, 2016; Cui and Schubert, 2017; Cui and Schubert, 2018; Hare et al., 2018). Our results contrast greatly with the reported hyperbolic Δ_{leaf} – pCO_2 relationship. Modern growth chamber studies demonstrate that Δ_{leaf} can respond to pCO_2 on timescales of weeks to months. However, when pCO_2 varies over millennial and longer timescales, plants adapt their leaf gas-exchange properties by changing the size and density of their stomata to optimize C assimilation and minimize water loss (i.e., water use efficiency) (Beerling and Woodward, 1995; Seibt et al., 2008; Franks and Beerling, 2009). Importantly, leaf physical parameters, such as stomatal density, are fixed for a given leaf and must be modified across multiple leaf generations (Šantrůček et al., 2014; Reichgelt et al., 2016). These physiological and biochemical responses over evolutionary timescales likely explain the large differences between this study and short-term experiments.

The transition in mechanistic response to pCO_2 likely starts occurring between subannual to decadal timescales (Lammertsma et al., 2011). For example, free-air CO_2 enrichment experiments carried out over 4–5 years find that assimilation increases and stomatal conductance decreases under elevated CO_2, resulting in no apparent change in plant c_i/c_a ratios (Ainsworth and Long, 2005), with c_i/c_a ratios being proportional to Δ_{leaf} in the simplest of physiological models of Δ_{leaf} (Farquhar et al., 1989; Cernusak et al., 2013). On decadal timescales, multiple studies have documented that plants respond to changing pCO_2 by adjusting stomatal size and density and by regulating the rate of carbon fixation to maintain optimal set points, including c_i to c_a concentrations (Woodward, 1987; Ehleringer and Cerling, 1995; Woodward and Kelly, 1995; Franks and Beerling, 2009; Franks et al., 2014). We suggest Δ_{leaf} cannot reliably be used as a pCO_2 proxy over geologic timescales, given that we observed a small negative relationship with pCO_2 during the early Cenozoic; this geologic reconstruction contrasts starkly with the positive relationships in select growth chamber studies used to generate the hyperbolic $\Delta_{leaf} - pCO_2$ function currently being applied to estimate pCO_2 (see also Diefendorf et al., 2015a; Kohn, 2016; Lomax et al., 2019; Zhang et al., 2019).

4.2. Δ_{leaf} sensitivity to other factors

4.2.1. Water availability

Modern global compilations of C_3 plants show that water availability is a strong predictor of Δ_{leaf} values (Diefendorf et al., 2010; Kohn, 2010). When plotted against a modern Δ_{leaf} compilation from Diefendorf et al. (2010), our paleo Δ_{leaf} values show good agreement with the average Δ_{leaf} – MAP relationship (Fig. 5). Only one site (Pitch Pinnacle) lies outside of the 90% confidence interval. This suggests paleo Δ_{leaf} is responding to environmental conditions over time similar to the way modern plants respond to spatial environmental variability. Though variability in Δ_{leaf} among sites may be influenced by factors other than MAP, such as plant type and altitude (e.g., Körner et al., 1988; Diefendorf et al., 2015b), precipitation appears to be an important factor for reconstructed Δ_{leaf} values. For example, the Florissant site has the second lowest Δ_{leaf} value (17.3‰) and the lowest MAP (647 +/–189 mm/yr) whereas the Stenkul Fiord site has the highest Δ_{leaf} value (24.6‰) and the highest MAP ($2400 + 104/-72$ mm/yr). While the relationship between MAP and Δ_{leaf} for our fossil sites ($R^2 = 0.39$; Pitch Pinnacle omitted) is weaker than that for modern woody C_3 plants ($R^2 = 0.55$), this could be due to the inherently large errors associated with measuring precipitation from fossil leaves. Preservation of paleoflora sites is also biased towards wetter sites, where high groundwater levels and surface water sources are required to preserve leaf fossils and organic matter. In addition, the relationship between MAP and Δ_{leaf} diminishes above 1500 mm/yr based on modern studies (Diefendorf et al., 2010; Kohn, 2010). Therefore, it should be expected that sampling mostly wet sites would minimize the effect of water availability on Δ_{leaf}. Given the large range in floral composition, MAT, and pCO_2 across this 40 myr suite of sites, it is remarkable that the reconstructed Δ_{leaf} – MAP relationship is so consistent with the relationship observed for modern woody plants (Fig. 5). Under the right conditions, such as controlling for differences in plant taxa and photosynthetic pathway, Δ_{leaf} is likely a reasonable indicator of water availability in geologic sediments (e.g., Diefendorf et al., 2010; Kohn, 2010).

4.2.2. Vegetation

Δ_{leaf} values are also sensitive to changes in vegetation. For instance, modern conifers have on average 2.7‰ lower Δ_{leaf} values than angiosperms growing at the same site due to differences in growth strategies and water use efficiency (e.g., Leavitt and Newberry, 1992; Murray et al., 1998; Diefendorf et al., 2010). Targeting paleoflora sites with well-preserved fossil leaves allows us to select sites with abundant angiosperms. In addition, both fossil leaves and *n*-alkanes are sourced from the upper canopy woody vegetation due to a taphonomic bias towards sun leaves (Greenwood, 1992; Graham et al., 2014; Freimuth et al., 2019). Most of our paleoflora sites are reconstructed as subtropical or temperate broadleaf and mixed forests dominated by angiosperms. However, during the Paleocene and Eocene, in some regions, such as the Arctic, deciduous conifers were locally abundant (McIver and Basinger, 1999; Eberle and Greenwood, 2012), and other sites also have conifer fossils (e.g., Driftwood Canyon, Falkland, Bighorn Basin sites, Florissant, Pitch Pinnacle). These nuances in vegetation type can be important when certain types of conifers are present at a site or when conifers are the dominant taxa due to differences in Δ_{leaf} values. For example, angiosperms generally produce significantly (up to 200 times) more *n*-C_{29} alkanes than most conifers that grow today and that lived during the early Cenozoic in North America

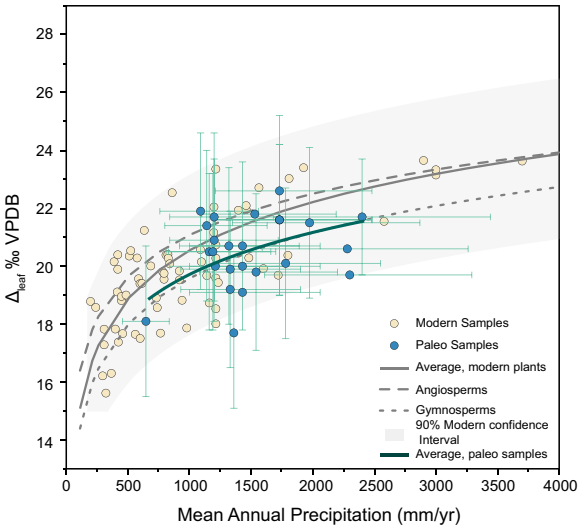

Fig. 5. A compilation of modern (Diefendorf et al., 2010) and paleo (this study) Δ_{leaf} values as a function of mean annual precipitation (MAP). For modern samples, each point represents a site-averaged mean. For paleo samples, each point represents a site-averaged mean from sediment samples collected along laterally continuous fossil-bearing units. Error bars for Δ_{leaf} represent combined uncertainty determined using Monte Carlo (see Fig. 4). Error bars for MAP represent the standard errors reported in Table 1. Paleo MAP values were determined at each locality from leaf area analysis (LAA) or climate leaf analysis multivariate program (CLAMP). Gray lines represent multiple linear regression analysis models of modern Δ_{leaf} – MAP for angiosperms (long dashed line), gymnosperms (short dashed line), and all samples (solid gray line). The shaded gray region represents the 90% confidence intervals for all modern samples. The dark blue-green line represent the multiple regression analysis model for the paleo Δ_{leaf} – MAP relationship, where Δ_{leaf} is equal to 5.5–4.8(Log_{10}-MAP) and $R^2 = 0.33$ for all sites. This relationship is in good agreement with modern Δ_{leaf} values in response to water availability.

(Pinaceae and taxodioids), with the exception of rare Podocarpaceae (Diefendorf et al., 2011; 2015b). We investigated the potential effects of increased conifer contribution on the $\Delta_{leaf} - pCO_2$ relationship by first documenting the groups of conifers at each site based on fossil leaf evidence, then assessing their n-C_{29} alkane production based on nearest living relatives (Diefendorf et al., 2015b) (Table 3).

Leaf fossil evidence at Axel Heiberg and Ellesmere island sites in the Canadian Arctic indicate that the most abundant conifers are the taxodioid Cupressaceae, *Metasequoia* and *Glyptostrobus*, with less frequent occurrences of other Cupressaceae and Pinaceae (Greenwood and Basinger, 1994; McIver and Basinger, 1999; Eberle and Greenwood, 2012; West et al., 2015; West et al., 2019). Conifers found at Driftwood Canyon include the taxodioid Cupressaceae *Metasequoia* and *Sequoia*, other Cupressaceae such as *Chamaecyparis* and *Thuja,* as well as diverse Pinaceae (Eberle et al., 2014). Conifers at Falkland include the taxodioid Cupressaceae *Metasequoia*, *Glyptostrobus, Taxodium*, and *Sequoia*, other Cupressaceae such as *Chamaecyparis,* and diverse Pinaceae (Smith et al., 2012). *Metasequoia* and *Glyptostrobus* are present at Bighorn Basin sites (Diefendorf et al., 2014). Conifers at Florissant include the Cupressaceae *Sequoia* and *Chamaecyparis* as well as *Torreya* from the Taxaceae family, and Pinaceae genera *Abies*, *Picea*, and *Pinus* (Gregory, 1994; Manchester, 2001). Pitch Pinnacle also has the Pinaceae genera *Abies*, *Picea*, and *Pinus*, as well as the Cupressaceae, *Juniperus* (Gregory and McIntosh, 1996).

Based on modern studies of n-alkane production in conifers, the genera of conifers at these sites are unlikely to be contributing significant amounts of n-C_{29} alkanes to the sediment (Diefendorf et al., 2015b). In modern individuals, the taxodioids *Metasequoia* and *Glyptostrobus* produce n-C_{29} and n-C_{31} alkanes at much lower concentrations compared to angiosperms. *Taxodium* and *Sequoia* are also taxodioids and produce low concentrations of all n-alkanes. *Chamaecyparis* produces n-alkane concentrations as high as angiosperms, but at significantly longer chain lengths (C_{33} and C_{35}). This preference for longer chain lengths is a conservative pattern across all Cupressoideae. As such, *Juniperus* and *Thuja*, also Cupressoideae, can make significant concentrations of n-alkanes, but predominantly at these longer chain lengths (C_{33} and C_{35}). *Torreya*, of the Taxaceae, produce low concentrations of n-alkanes. Additionally, all genera of Pinaceae produce very low concentrations of n-alkanes.

Given that several sites have conifers that could have been contributing some small amount of n-C_{29} and n-C_{31} alkanes to the sediments, we cannot preclude that these conifer-derived n-alkanes are not influencing Δ_{leaf}, at least to some degree. Because conifer-derived Δ_{leaf} values are ~2.7‰ lower than angiosperms (Diefendorf et al., 2010), we tested how changes in vegetation might affect our observed $\Delta_{leaf} - pCO_2$ relationship. At sites with notable conifer evidence (Ellesmere and Axel Heiberg island sites, Driftwood Canyon, Falkland, Florissant, and Pitch Pinnacle), we assumed the $n$$C_{29}$-alkanes were 100% conifer-derived as an extreme end member and added 2.7‰ to the average Δ_{leaf} values of each site, representing a maximum 'angiosperm correction'. The Bighorn Basin sites were excluded from this correction based on several studies indicating n-alkanes preserved at these sites are angiosperm-derived (Diefendorf et al., 2014; Diefendorf et al., 2015a). We then performed a multiple regression analysis with pCO_2 and MAP and found pCO_2 has no correlation with Δ_{leaf} ($p = 0.656$, $n = 26$, $R^2 = 0.10$). This suggests that the presence of conifers could influence Δ_{leaf} and overprint the observed $\Delta_{leaf} - pCO_2$ relationship. It is important to note that this exercise demonstrates the effects of extreme vegetation end members and is not realistic. For our sites, it is highly unlikely that $n$$C_{29}$-alkanes are exclusively conifer-derived based on the genera present at each site (see Table 3) and vegetation likely has a minimal influence on the $\Delta_{leaf} - pCO_2$ relationship (Fig. 4).

4.2.3. Altitude

Compared to our lower elevation sites (Big Cedar Ridge, Kaiparowits, Arctic sites), a number of paleoflora localities have higher paleoelevations (>1 km), such as Driftwood Canyon (0.8–1 km), Falkland (1.3 km), Florissant (1–3 km), and Pitch Pinnacle (2–3 km) (Gregory and

Mcintosh, 1996; Meyer, 2001; Smith et al., 2009; Zaborac-Reed and Leopold, 2016). Modern studies have demonstrated a strong negative correlation between elevation and Δ_{leaf} (Körner et al., 1988; Wu et al., 2017; Feakins et al., 2018). For example, Wu et al. (2017) observed a 1‰/km decrease in Δ_{leaf} values with increasing altitude in a tropical forest transect in South America. Therefore, elevation might influence Δ_{leaf} values for higher elevation sites. For instance, Pitch Pinnacle has the highest paleoelevation and the lowest Δ_{leaf} values despite having a moderate MAP. However, altitude estimates are not available for all sites and, when given, are prone to a wide range of uncertainty based on the various paleoelevation methods and proxies (Zaborac-Reed and Leopold, 2016). Therefore, altitude was not included in statistical analyses. Rather, sites with higher elevations (>1 km; Driftwood Canyon, Falkland, Florissant, and Pitch Pinnacle) were removed, to test the $\Delta_{leaf} - pCO_2$ relationship for sites with similar altitude, with an additional multiple linear regression analysis. We find that pCO_2 maintains a negative effect on Δ_{leaf} ($p < 0.0001$), while MAP has no effect ($p = 0.34$) on Δ_{leaf} (Supplementary Data 1; Table 2). The decrease in explanatory power of MAP is not unexpected because the higher elevation sites are also the dryer sites.

4.3. Leaf gas-exchange dynamics from the Late Cretaceous to Oligocene

In our North American dataset, we find that site-averaged Δ_{leaf} decreases by 2.1‰ from 200 to 900 ppmV of pCO_2 for all sites after accounting for MAP. Modeling studies, theory, and other observations have used Δ_{leaf} to infer changes in leaf gas-exchange strategies over time (e.g., Ehleringer and Cerling, 1995; Franks and Beerling, 2009; Voelker et al., 2016). Using the model developed by Farquhar et al. (1989) (see Eq. (1)), Δ_{leaf} is often used to derive the c_i/c_a ratio to investigate how plants modify leaf gas-exchange strategies to changing pCO_2 (Farquhar and Sharkey, 1982; Ehleringer and Cerling, 1995; Franks and Beerling, 2009; Voelker et al., 2016). The c_i/c_a ratio represents the balance between rates of stomatal conductance (g_c) and CO_2 assimilation (A) via Fick's Law ($A = g_c (c_a - c_i)$). To modify g_c on long timescales, plants alter their stomatal size and density (Franks and Beerling, 2009). Plants can modify net A by adjusting the maximum carboxylation rates of Rubisco. Assimilation rates are tied to phylogeny, growth form, and solar exposure in an environment (Reichgelt and D'Andrea, 2019), as well as nitrogen availability (Wullschleger, 1993; Franks and Beerling, 2009; Voelker et al., 2016). As pCO_2 changed over geologic time, it is thought that plants adjusted g_c, maximum carboxylation rates, and other traits in a manner that maximizes carbon gain during photosynthesis while minimizing water loss from transpiration (Ehleringer and Cerling, 1995; Seibt et al., 2008; Franks et al., 2013).

There are a number of possible leaf gas-exchange strategies for adapting to changes in pCO_2, such as maintaining constant c_i values, maintaining constant $c_a - c_i$ values, maintaining constant c_i/c_a ratios, or by shifting between these strategies (Seibt et al., 2008; Voelker et al., 2016). Each strategy implies different physiological and evolutionary responses of leaf gas-exchange to pCO_2. For instance, maintaining a constant c_i value as c_a increases would require a plant to significantly increase A and/or decrease g_c. Preserving constant $c_a - c_i$ values would require comparatively smaller adjustments to A and/or g_c and a constant c_i/c_a ratio indicates intermediate modifications (Voelker et al., 2016). Our data implies that both c_i and $c_a - c_i$ increase with rising pCO_2, while the c_i/c_a ratio decreases slightly from 0.80 to 0.59 across 700 ppmV (Fig. 6).

Negative $c_i/c_a - pCO_2$ relationships have been recorded in a few centennial-scale modern studies and are attributed to increased intrinsic water use efficiency (iWUE) (Ehleringer and Cerling, 1995; Giguère-Croteau et al., 2019). Ehleringer and Cerling (1995) observed a decreasing c_i/c_a ratio and constant c_i with increasing pCO_2 in Atacama leaf litter samples and proposed that these trees were maintaining a constant photosynthetic rate by increasing iWUE.

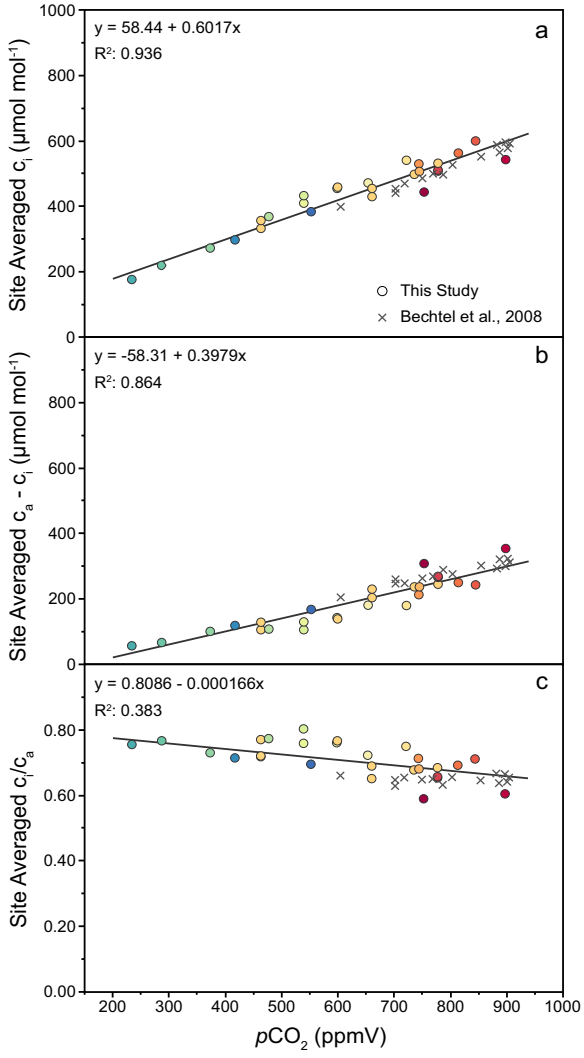

Fig. 6. Site-averaged leaf gas-exchange relationships for each paleoflora site derived from Δ_{leaf} (Eq. (1)) as a function of proxy-based pCO_2 estimates from Foster et al. (2017). Panel (a) is the c_a values. Panel (b) is the $c_a - c_i$ values. Panel (c) is the c_i/c_a ratios.

This could have been accomplished by decreasing g_c to prevent stomatal water loss. Using tree ring data, Giguère-Croteau et al. (2019) observed a negative $c_i/c_a - pCO_2$ relationship and a neutral then positive shift in c_i with rising pCO_2, also attributing these trends to increased iWUE. Our data show a gradual decrease in c_i/c_a ratios and an increase in c_i with rising pCO_2.

Our study seems to indicate that c_i is increasing, but at a slower rate than c_a, leading to an overall decrease in the c_i/c_a ratio. However, these observations do not directly coincide with the models proposed by Voelker et al. (2016) or the long-term c_i observations made by Ehleringer and Cerling, (1995) and Giguère-Croteau et al. (2019). It is possible that long-term changes of leaf gas-exchange properties at the species level do not directly translate to ecosystem scale, as represented in the paleorecord. However, lack of a large apparent response of Δ_{leaf} to pCO_2 in the paleorecord does suggest leaf gas-exchange properties, such as stomatal conductance and assimilation, are both modified to some extant in response to pCO_2, perhaps to maximize iWUE as suggested in previous studies (Seibt et al., 2008; Franks and Beerling, 2009; Frank et al., 2015).

4.4. Trends in Δ_{leaf} through time

Our statistical analyses show that some but not all of the 4.9‰ spread in Δ_{leaf} values can be attributed to shifts in pCO_2 and MAP during this time period. Beginning with the radiation and diversification of angiosperms during the Cretaceous (Wing and Boucher, 1998), a number of major climatic and vegetation changes occurred over this 40 myr period, and these changes could have impacts on Δ_{leaf} that are additional to, or coincident with, the impacts of shifts in MAP and pCO_2. For example, a bolide impact marking the Cretaceous-Paleogene (K-Pg) boundary (66 myr) was associated with high plant extinction and large floral turnover in the Paleocene, concurrent with global cooling (Wilf et al., 2003; Wilf and Johnson, 2004). Following this impact event, the earliest Paleocene recovery flora was generally low in diversity and dominated by angiosperms with evidence for a large scale shift in plant ecological strategies from the Cretaceous to the Paleocene (e.g., Vajda and Bercovici, 2014). Blonder et al. (2014) showed that leaves increased their vein density and decreased their leaf mass per area across the K-Pg boundary, evidence for "fast-return" leaves that have shorter lifespans and prioritize carbon assimilation and low tissue carbon investment. It is then possible that these early Paleocene angiosperm taxa were prioritizing carbon gain over water use efficiency, which could have resulted in higher Δ_{leaf} values. Paleoflora evidence also indicates many locations had high precipitation in the early Paleocene (Uhl et al., 2007; Greenwood et al., 2010; Geng et al., 2018) which may also explain, to some extent, high Δ_{leaf} values in our dataset during this time (SJB Pu2 and Arctic sites).

Abrupt warming during the Paleocene-Eocene Thermal Maximum (PETM) also resulted in major changes in flora composition across North America (Smith et al., 2007; Wing and Currano, 2013; Willard et al., 2019), though post-PETM plant composition was similar to pre-PETM conditions. During the late Paleocene and early Eocene, we observe that Δ_{leaf} values remain elevated. The Early Eocene Climatic Optimum (EECO) was also marked by warm, wet conditions and more seasonal precipitation (Wing and Greenwood, 1993), consistent with modern studies that show a strong trend between high water availability and high Δ_{leaf} values (Kohn, 2010). Global cooling and drying occurred through the late Eocene and Oligocene (Wing, 1987; Zachos et al., 2001). We observe that Δ_{leaf} values gradually decrease through the Eocene, reaching their lowest in the Oligocene; this could reflect the transition from subtropical vegetation (potentially higher Δ_{leaf}) to temperate mixed coniferous and broad-leaved deciduous flora (potentially lower Δ_{leaf}) in response to global cooling and drying. In modern studies, deciduous angiosperms tend to have lower Δ_{leaf} values than evergreen angiosperms (Diefendorf et al., 2010), though phylogenetic differences among genera may be more important than leaf lifespan on Δ_{leaf} (Diefendorf et al., 2015b). As Δ_{leaf} decreases in the late Eocene and Oligocene, plants may have been increasing their iWUE in response to drier conditions, as indicated by the shift to temperate, deciduous vegetation. Though our samples from paleoflora sites represent much lower temporal resolution than continuous records, such as marine cores, Δ_{leaf} seems to be responding to large-scale trends in water availability in response to climate and vegetation change on geologic timescales and is not strongly influenced by pCO_2 because of these complex feedbacks.

5. CONCLUSIONS

Based on leaf wax *n*-alkanes in sediments from 26 sites that span 40 million years, the estimated Δ_{leaf} values and c_i/c_a ratios show a gradual decline (Fig. 4; Fig. 6) from ~230 to 900 ppmV of pCO_2. After accounting for MAP using a multiple regression analysis, we found a negative correlation between Δ_{leaf} and pCO_2 (-0.3 ± 0.09‰/100 ppmV) which is very similar to, but more pronounced than, the findings of Kohn (2016) and differs from most growth chamber experiments (i.e., Schubert and Jahren, 2012). We also find that Δ_{leaf} values show good agreement with modern Δ_{leaf} – MAP relationships (Fig. 5; Diefendorf et al., 2010; Kohn, 2010). Based on these results, Δ_{leaf} values are responding to water availability and pCO_2, and to a lesser extent, vegetation and possibly altitude in the geologic record.

Together, MAP and pCO_2 explain ~49% of the variability in Δ_{leaf} values in our data. However, the effects of vegetation type and altitude may play a role and should also be the focus of future work. Based on these observations, we argue that the relationship between Δ_{leaf} and pCO_2 is not robust enough on million-year timescales for Δ_{leaf} to be an effective pCO_2 proxy, especially if factors such as precipitation, vegetation, or altitude are not taken into account. The small (-0.3 ± 0.09‰/100 ppmV) response of Δ_{leaf} to changing pCO_2 seems to support leaf stomata studies (Beerling and Woodward, 1997; Beerling and Royer, 2002; Franks and Beerling, 2009) that show on these long timescales, plants change the size and density of their stomata, and likely other properties, thus optimizing leaf gas exchange to maximize C gain and minimize water loss with

increasing pCO_2. Furthermore, the relationship between Δ_{leaf} and MAP in our paleo samples were similar to the observed relationship in modern plants (Diefendorf et al., 2010; Kohn, 2010), suggesting plants have been adapting and responding to water availability in similar ways since at least the Late Cretaceous.

RESEARCH DATA

Schlanser, Kristen M; Diefendorf, Aaron F; Greenwood, David R; Mueller, Kevin E; West, Christopher K; Lowe, Alexander J; Basinger, James F; Currano, Ellen D; Flynn, Andrew G; Fricke, Henry C; Geng, Jie; Meyer, Herbert W; Peppe, Daniel J (2019): Leaf wax n-alkane carbon isotope data from sediment samples collected from fossil leaf sites extending from New Mexico to the High Arctic. PANGAEA, https://doi.org/10.1594/PANGAEA.909151.

Declaration of Competing Interest

The authors declare that they have no known competing financial interests or personal relationships that could have appeared to influence the work reported in this paper.

ACKNOWLEDGEMENTS

We thank Sarah Feakins and three anonymous reviewers for helfpul comments that improved this manuscript. We thank Erika Freimuth, Yeon Jee Suh, and Scott Wing for stimulating discussions. We also thank Hans Naake, Megan Brennan, and Jed Ball for assistance with sample preparation. We thank Talia Karim at the Colorado University Museum of Natural History and Conni O'Connor at Florissant Fossil Beds National Monument for assistance with museum specimen sample collection. For Driftwood Canyon, Falkland and the High Arctic sites, David R. Greenwood, James F. Basinger and Christopher K. West acknowledge the assistance of various field party members in the collection of samples over several years. Field work on Axel Heiberg and Ellesmere islands involved logistical support from the Polar Continental Shelf Project. Christopher K. West thanks Lutz Reinhardt and Karsten Piepjohn of the Bundesanstalt für Geowissenschaften und Rohstoffe (BGR) [Federal Institute for Geosciences and Natural Resources] for funding and logistics in support of field work on Ellesmere Island. Work at Driftwood Canyon and High Arctic sites was under permits issued by the governments British Columbia and Nunavut respectively. For the San Juan Basin site, we thank Tom Williamson, Brittany Abbuhl, Parker Wright, Joe Milligan, Ross Secord, Stephen Brusatte, Utanah Denenclaw, Caitlin Leslie, Adam Davis, Stacy Atchley, Aly Baumgartner, and Anne Weil for assistance in the field and lab. This research was supported by the U.S. National Science Foundation (EAR-1229114 and EAR-1636740 to AFD; EAR-132552 to DJP), the American Chemical Society Petroleum Research Fund (PRF#52822-DN18 to DJP), the Natural Sciences and Engineering Research Council of Canada (to DRG and JFB), the Geological Society of America, Dallas Paleontological Society, and Baylor University Department of Geosciences' Dixon Fund.

APPENDIX A. SUPPLEMENTARY MATERIAL

Supplementary data to this article can be found online at https://doi.org/10.1016/j.gca.2019.11.023.

REFERENCES

Ainsworth E. A. and Long S. P. (2005) What have we learned from 15 years of free-air CO2 enrichment (FACE)? A meta-analytic review of the responses of photosynthesis, canopy properties and plant production to rising CO2. *New Phytol.* **165**, 351–372.

Allen S. E., Lowe A. J., Peppe D. J. and Meyer H. W. (2017) Paleoclimate and paleoecology of the late Eocene Florissant flora using digital leaf physiognomy. *Geol. Soc. Am. Abstracts Programs* **49**(6). https://doi.org/10.1130/abs/2017AM-305823.

Barral A., Gomez B., Legendre S. and Lécuyer C. (2017) Evolution of the carbon isotope composition of atmospheric CO2 throughout the Cretaceous. *Palaeogeogr. Palaeoclimatol. Palaeoecol.* **471**, 40–47.

Barton M. A. (2006) Floral diversity and climate change in central Colorado during the Eocene and Oligocene. (Masters Thesis) University of Colorado, Boulder, Colorado.

Battipaglia G., Saurer M., Cherubini P., Calfapietra C., Mccarthy H. R., Norby R. J. and Cotrufo M. F. (2013) Elevated CO2 increases tree-level intrinsic water use efficiency: insights from carbon and oxygen isotope analyses in tree rings across three forest FACE sites. *New Phytol.* **197**, 544–554.

Bechtel A., Gratzer R., Sachsenhofer R. F., Gusterhuber J., Lücke A. and Püttmann W. (2008) Biomarker and carbon isotope variation in coal and fossil wood of Central Europe through the Cenozoic. *Palaeogeogr. Palaeoclimatol. Palaeoecol.* **262**, 166–175.

Becklin K. M., Medeiros J. S., Sale K. R. and Ward J. K. (2014) Evolutionary history underlies plant physiological responses to global change since the last glacial maximum. *Ecol. Lett.* **17**, 691–699.

Beerling D. J. and Royer D. L. (2002) Reading a CO2 signal from fossil stomata. *New Phytol.* **153**, 387–397.

Beerling D. J. and Woodward F. I. (1997) Changes in land plant function over the phanerozoic: reconstructions based on the fossil record. *Bot. J. Linn. Soc.* **124**, 137–153.

Beerling D. J. and Woodward F. I. (1993) Ecophysiological responses of plants to global environmental change since the Last Glacial Maximum. *New Phytol.* **125**, 641–648.

Beerling D. J. and Woodward F. I. (1995) Leaf stable carbon isotope composition records increased water-use efficiency of C3 plants in response to atmospheric CO2 enrichment. *Funct. Ecol.* **9**, 394–401.

Blonder B., Royer D. L., Johnson K. R., Miller I. and Enquist B. J. (2014) Plant ecological strategies shift across the Cretaceous-Paleogene boundary. *PLoS Biol.* **12**, 1–7.

Bush R. T. and McInerney F. A. (2013) Leaf wax n-alkane distributions in and across modern plants: implications for paleoecology and chemotaxonomy. *Geochim. Cosmochim. Acta* **117**, 161–179.

Bush R. T. (2014) Leaf wax n-alkanes as paleoclimate proxies: calibrations in modern plants and applications in ancient ecosystems. (PhD Dissertation). Northwestern University, Evanston, IL.

Cernusak L. A., Ubierna N., Winter K., Holtum J. A. M., Marshall J. D. and Farquhar G. D. (2013) Environmental and physiological determinants of carbon isotope discrimination in terrestrial plants. *New Phytol.* **200**, 950–965.

Coplen T. B., Brand W. A., Gehre M., Gröning M., Meijer H. A., Toman B. and Verkouteren R. M. (2006) New guidelines for δ13C measurements. *Anal. Chem.* **78**, 2439–2441.

Cui Y. and Schubert B. A. (2017) Atmospheric pCO2 reconstructed across five early Eocene global warming events. *Earth Planet. Sci. Lett.* **478**, 225–233.

Cui Y. and Schubert B. A. (2018) Towards determination of the source and magnitude of atmospheric pCO2 change across the

early Paleogene hyperthermals. *Glob. Planet. Change* **170**, 120–125.

Cui Y. and Schubert B. A. A. (2016) Quantifying uncertainty of past pCO2 determined from changes in C3 plant carbon isotope fracitionation. *Geochim. Cosmochim. Acta* **176**, 127–138.

Currano E. D., Pinheiro E. R. S., Buchwaldt R., Clyde W. C. and Miller I. M. (2019) Endemism in Wyoming plant and insect herbivore communities during the early Eocene hothouse. *Paleobiology* **45**, 421–439.

Davies-Vollum K. S. and Wing S. L. (1998) Sedimentological, taphonomic, and climatic aspects of Eocene swamp deposits (Willwood Formation, Bighorn Basin, Wyoming). *Palaios* **13**, 28–40.

Diefendorf A. F., Freeman K. H. and Wing S. L. (2014) A comparison of terpenoid and leaf fossil vegetation proxies in Paleocene and Eocene Bighorn Basin sediments. *Org. Geochem.* **71**, 30–42.

Diefendorf A. F., Freeman K. H., Wing S. L., Currano E. D. and Mueller K. E. (2015a) Paleogene plants fractionated carbon isotopes similar to modern plants. *Earth Planet. Sci. Lett.* **429**, 33–44.

Diefendorf A. F., Freeman K. H., Wing S. L. and Graham H. V. (2011) Production of n-alkyl lipids in living plants and implications for the geologic past. *Geochim. Cosmochim. Acta* **75**, 7472–7485.

Diefendorf A. F. and Freimuth E. J. (2017) Extracting the most from terrestrial plant-derived n-alkyl lipids and their carbon isotopes from the sedimentary record: a review. *Org. Geochem.* **103**, 1–21.

Diefendorf A. F., Leslie A. B. and Wing S. L. (2015b) Leaf wax composition and carbon isotopes vary among major conifer groups. *Geochim. Cosmochim. Acta* **170**, 145–156.

Diefendorf A. F., Mueller K. E., Wing S. L., Koch P. L. and Freeman K. H. (2010) Global patterns in leaf 13C discrimination and implications for studies of past and future climate. *Proc. Natl. Acad. Sci. USA* **107**, 5738–5743.

Eberle J. J. and Greenwood D. R. (2012) Life at the top of the greenhouse Eocene world – a review of the Eocene flora and vertebrate fauna from Canada's High Arctic. *Bull. Geol. Soc. Am.* **124**, 3–23.

Eberle J. J., Rybczynski N., Greenwood D. R. and Taylor P. (2014) Early Eocene mammals from the Driftwood Creek beds, Driftwood Canyon Provincial Park, northern British Columbia. *J. Vertebr. Paleontol.* **34**, 739–746.

Ehleringer J. R. and Cerling T. E. (1995) Atmospheric CO2 and the ratio of intercellular to ambient CO2 concentrations in plants. *Tree Physiol.* **15**, 105–111.

Evanoff E., McIntosh W. C. and Murphey, P. C. (2001) Stratigraphical summary and 40Ar/39Ar geochronology of the Florissant Formation, Colorado. In: Evanoff, E., Gregory-Wodzicki K. M. and Johnson K. R. (Eds.) Fossil Flora and Stratigraphy of the Florissant Formation, Colorado, Proc. Denver Mus. Nat. Sci. 4, 1–16.

Farquhar G. D., Ehleringer J. R. and Hubick K. T. (1989) Carbon isotope discrimination and photosynthesis. *Ann. Rev. Plant Physiol.* **40**, 503–537.

Farquhar G. D. and Richards R. A. (1984) Isotopic composition of plant carbon correlates with water-use efficiency of wheat genotypes. *Aust. J. Plant Physiol.* **11**, 539–552.

Farquhar G. D. and Sharkey T. D. (1982) Stomatal conductance and photosynthesis. *Annu. Rev. Plant Physiol.* **33**, 317–345.

Feakins S. J., Wu M. S., Ponton C., Galy V. and West A. J. (2018) Dual isotope evidence for sedimentary integration of plant wax biomarkers across an Andes-Amazon elevation transect. *Geochim. Cosmochim. Acta* **242**, 64–81.

Flynn A. G. amd Peppe D. P. (In press) Early Paleocene tropical forest from the Ojo Alamo Sandstone, San Juan Basin, New Mexico, USA, *Paleobiology*, pp. 1–24., 10.1017/pab.2019.24.

Foster G. L., Royer D. L. and Lunt D. J. (2017) Future climate forcing potentially without precedent in the last 420 million years. *Nat. Commun.* **8**, 14845.

Frank D. C., Poulter B., Saurer M., Esper J., Huntingford C., Helle G., Treydte K., Zimmermann N. E., Schleser G. H., Ahlström A., Ciais P., Friedlingstein P., Levis S., Lomas M., Sitch S., Viovy N., Andreu-Hayles L., Bednarz Z., Berninger F., Boettger T., D'Alessandro C. M., Daux V., Filot M., Grabner M., Gutierrez E., Haupt M., Hilasvuori E., Jungner H., Kalela-Brundin M., Krapiec M., Leuenberger M., Loader N. J., Marah H., Masson-Delmotte V., Pazdur A., Pawelczyk S., Pierre M., Planells O., Pukiene R., Reynolds-Henne C. E., Rinne K. T., Saracino A., Sonninen E., Stievenard M., Switsur V. R., Szczepanek M., Szychowska-Krapiec E., Todaro L., Waterhouse J. S. and Weigl M. (2015) Water-use efficiency and transpiration across European forests during the Anthropocene. *Nat. Clim. Change.* **5**, 579–583.

Franks P. J., Adams M. A., Amthor J. S., Barbour M. M., Berry J. A., Ellsworth D. S., Farquhar G. D., Ghannoum O., Lloyd J., Mcdowell N., Norby R. J., Tissue D. T. and von Caemmerer S. (2013) Sensitivity of plants to changing atmospheric CO2 concentration: from the geological past to the next century. *New Phytol.* **197**, 1077–1094.

Franks P. J. and Beerling D. J. (2009) CO2-forced evolution of plant gas exchange capacity and water-use efficiency over the Phanerozoic. *Geobiology* **7**, 227–236.

Franks P. J., Royer D. L., Beerling D. J., Van de Water P. K., Cantrill D. J., Barbour M. M. and Berry J. A. (2014) New constraints on atmospheric CO2 concentration for the Phanerozoic. *Geophys. Res. Lett.* 41, 4685–4694.

Freimuth E. J., Diefendorf A. F., Lowell T. V. and Wiles G. C. (2019) Sedimentary n-alkanes and n-alkanoic acids in a temperate bog are biased toward woody plants. *Org. Geochem.* **128**, 94–107.

Geng J., Flynn A. G. and Peppe D. J. (2018) Paleoclimate reconstruction and pattern of climate change at Early Paleocene from leaf physiognomy at San Juan Basin, New Mexico following the Cretaceous-Paleogene Boundary. Geol. Soc. Am. Abstracts Programs, 50(6). 10.1130/abs/2018AM-322923.

Giguère-Croteau C., Boucher É., Bergeron Y., Girardin M. P., Drobyshev I., Silva L. C. R., Hélie J.-F. and Garneau M. (2019) North America's oldest boreal trees are more efficient water users due to increased [CO2], but do not grow faster. *Proc. Natl. Acad. Sci. USA* **116**, 2749–2754.

Graham H. V., Patzkowsky M. E., Wing S. L., Parker G. G., Fogel M. L. and Freeman K. H. (2014) Isotopic characteristics of canopies in simulated leaf assemblages. *Geochim. Cosmochim. Acta* **144**, 82–95.

Greenwood D. R. (1992) Taphonomic constraints on foliar physiognomic interpretations of Late Cretaceous and Tertiary palaeoclimates. *Rev. Palaeobot. Palynol.* **71**, 149–190.

Greenwood D. R., Archibald S. B., Mathewes R. W. and Moss P. T. (2005) Fossil biotas from the Okanagan Highlands, southern British Columbia and northeastern Washington State: climates and ecosystems across an Eocene landscape. *Can. J. Earth Sci.* **42**, 167–185.

Greenwood D. R. and Basinger J. F. (1994) The paleoecology of high-latitude Eocene swamp forests from Axel Heiberg Island, Canadian High Arctic. *Rev. Palaeobot. Palynol.* **81**, 83–97.

Greenwood D. R., Basinger J. F. and Smith R. Y. (2010) How wet was the Arctic Eocene rain forest? Estimates of precipitation from Paleogene Arctic macrofloras. *Geology* **38**, 15–18.

Gregory K. M. (1994) Palaeoclimate and palaeoelevation of the 35 Ma Florissant flora, Front Range, Colorado. *Palaeoclimates* **1**, 23–57.

Gregory K. M. and Mcintosh W. C. (1996) Paleoclimate and paleoelevation of the Oligocene Pitch-Pinnacle flora, Sawatch Range, Colorado. *GSA Bull.* **108**, 545–561.

Hare V. J., Loftus E., Jeffrey A. and Ramsey C. B. (2018) Atmospheric CO2 effect on stable carbon isotope composition of terrestrial fossil archives. *Nat. Commun.* **9**, 252.

Harrison J. C., Mayr U., McNeil D. H., Sweet A. R., McIntyre D. J., Eberle J. J., Harington C. R., Chalmers J. A., Dam G. and Nøhr-Hansen H. (1999) Correlation of Cenozoic sequences of the Canadian Arctic region and Greenland; implications for the tectonic history of northern North America. *Bull. Can. Pet. Geol.* **47**, 223–254.

Jahren A. H., Arens N. C. and Harbeson S. A. (2008) Prediction of atmospheric δ13CO2 using fossil plant tissues. *Rev. Geophys.* **46**, 1–12.

Kohn M. J. (2010) Carbon isotope compositions of terrestrial C3 plants as indicators of (paleo)ecology and (paleo)climate. *Proc. Natl. Acad. Sci. USA* **107**, 19691–19695.

Kohn M. J. (2016) Carbon isotope discrimination in C3 land plants is independent of natural variations in pCO2. *Geochemical Perspect. Lett.* **2**, 35–43.

Körner C., Farquhar G. D. and Roksandic Z. (1988) A global survey of carbon isotope discrimination in plants from high altitude. *Oecologia* **74**, 623–632.

Lammertsma E. I., Boer H. J. d., Dekker S. C., Dilcher D. L., Lotter A. F. and Wagner-Cremer F. (2011) Global CO2 rise leads to reduced maximum stomatal conductance in Florida vegetation. *Proc. Natl. Acad. Sci.* 108, 4035–4040.

Leakey A. D. B., Ainsworth E. A., Bernacchi C. J., Rogers A., Long S. P. and Ort D. R. (2009) Elevated CO2 effects on plant carbon, nitrogen, and water relations: six important lessons from FACE. *J. Exp. Bot.* **60**, 2859–2876.

Leavitt S. W. and Newberry T. (1992) Systemics of stable-carbon isotopic differences between gymnosperm and angiosperm trees. *Plant Physiol.* **11**, 257–262.

Leopold E. (1974) Pollen and spores of the Kissinger fossil leaf locality. In *An early Eocene Flora from the Yellowstone-Absaroka volcanic province, northwestern Wind River basin* (ed. H. D. MacGinitie). Wyoming, University of California Press, Berkeley, USA, pp. 49–66.

Lomax B. H., Lake J. A., Leng M. J. and Jardine P. E. (2019) An experimental evaluation of the use of Δ13C as a proxy for palaeoatmospheric CO2. *Geochim. Cosmochim. Acta* **247**, 162–174.

Manchester S. R. (2001) Update on the megafossil flora of Florissant, Colorado. In: E. Evanoff, K. Gregory-Wodzicki, and K. Johnson. (Eds.), Fossil flora and stratigraphy of the Florissant Formation, Colorado, *Proc. Denver Mus. Nat. Sci.* 4, 137–162.

Mason I. P. (2013) *40Ar/39Ar Chronostratigraphy of the late Cretaceous early Paleocene Rocks of the San Juan Basin, NM* (Masters Thesis). Baylor University, Waco, Texas.

McIver E. E. and Basinger J. F. (1999) Early tertiary floral evolution in the Canadian High Arctic. *Ann. Missouri Bot. Gard.* **86**, 523–545.

Meyer H. W. (2001) A review of the paleoelevation estimates for the Florissant flora. In: E. Evanoff, K. Gregory-Wodzicki, and K. Johnson. (Eds.), Fossil Flora and Stratigraphy of the Florissant Formation, Colorado, *Proc. Denver Mus. Nat. Sci.* 4, 205–216.

Miller I. M., Brandon M. T. and Hickey L. J. (2006) Using leaf margin analysis to estimate the mid-Cretaceous (Albian) paleolatitude of the Baja BC block. *Earth Planet. Sci. Lett.* **245**, 95–114.

Miller I. M., Johnson K. R., Kline D. E., Nichols D. J. and Barclay R. S. (2013) A late Campanian flora from the Kaiparowits Formation, Southern Utah, and a brief overview of the widely sampled but little-known Campanian vegetation of the Western Interior of North America. In *At the Top of the Grand Staircase* (eds. A. L. Titus and M. A. Loewen). Indiana University Press, Bloomington and Indianapolis, USA, pp. 107–131.

Moss P. T., Greenwood D. R. and Archibald S. B. (2005) Regional and local vegetation community dynamics of the Eocene Okanagan Highlands (British Columbia - Washington State) from palynology. *Can. J. Earth Sci.* **42**, 187–204.

Mueller K. E., Blumenthal D. M., Pendall E., Carillo Y., Dijkstra F. A., Williams D. G., Follett R. F., Morgan J. A., Carrillo Y., Dijkstra F. A., Williams D. G., Follett R. F. and Morgan J. A. (2016) Impacts of warming and elevated CO2 on a semi-arid grassland are non-additive, shift with precipitation, and reverse over time. *Ecol. Lett.* **19**, 956–966.

Murray A. P., Edwards D., Hope J. M., Boreham C. J., Booth W. E., Alexander R. A. and Summons R. E. (1998) Carbon isotope biogeochemistry of plant resins and derived hydrocarbons. *Org. Geochem.* **29**, 1199–1214.

Nowak R. S., Ellsworth D. S. and Smith S. D. (2004) Functional responses of plants to elevated atmospheric CO2 – do photosynthetic and productivity data from FACE experiments support early predictions? *New Phytol.* **162**, 253–280.

O'Leary M. H. (1981) Carbon isotope fractionation in plants. *Phytochemistry* **20**, 553–567.

Peppe D. J., Baumgartner A., Flynn A. and Blonder B. (2018) Reconstructing paleoclimate and paleoecology using fossil leaves. In *Methods in Paleoecology* (eds. D. Croft, D. Su and S. Simpson). Springer, Cham, Switzerland, pp. 289–317.

Polissar P. J., Freeman K. H., Rowley D. B., McInerney F. A. and Currie B. S. (2009) Paleoaltimetry of the Tibetan Plateau from D/H ratios of lipid biomarkers. *Earth Planet. Sci. Lett.* **287**, 64–76.

Porter A. S., Evans-Fitz.Gerald C., McElwain J. C., Yiotis C. and Elliott-Kingston C. (2015) How well do you know your growth chambers? Testing for chamber effect using plant traits. *Plant Methods* 11, 1–10.

Porter A. S., Evans-Fitz.Gerald C., Yiotis C., Montañez I. P. and McElwain J. C. (2019) Testing the accuracy of new paleoatmospheric CO2 proxies based on plant stable carbon isotopic composition and stomatal traits in a range of simulated paleoatmospheric O2:CO2 ratios. *Geochim. Cosmochim. Acta* 259, 69–90.

Porter A. S., Yiotis C., Montañez I. P. and McElwain J. C. (2017) Evolutionary differences in Δ13C detected between spore and seed bearing plants following exposure to a range of atmospheric O2:CO2 ratios; implications for paleoatmosphere reconstruction. *Geochim. Cosmochim. Acta* **213**, 517–533.

Reichgelt T. and D'Andrea W. J. (2019) Plant carbon assimilation rates in atmospheric CO2 reconstructions. *New Phytol.* **223**, 1844–1855.

Reichgelt T., D'Andrea W. J. and Fox B. R. S. (2016) Abrupt plant physiological changes in southern New Zealand at the termination of the Mi-1 event reflect shifts in hydroclimate and pCO2. *Earth Planet. Sci. Lett.* **455**, 115–124.

Reinhardt L., Estrada S., Andruleit H., Dohrmann R., Piepjohn K., von Gosen W., Davis D. W. and Davis B. (2013) Altered volcanic ashes in Palaeocene and Eocene sediments of the Eureka Sound Group (Ellesmere Island, Nunavut, Arctic Canada). *Z. Dt. Ges. Geowiss. (German J. Geosci.)* **164**(1), 131–147.

Reinhardt L., von Gosen W., Piepjohn K., Lückge A. and Schmitz M. (2017) The Eocene Thermal Maximum 2 (ETM-2) in a terrestrial section of the High Arctic: identification by U-Pb zircon ages of volcanic ashes and carbon isotope records of coal and amber (Stenkul Fiord, Ellesmere Island, Canada). *EGU General Assembly Conference Abstracts* **19**, 8145.

Šantrůček J., Vráblová M., Šimková M., Hronková M., Drtinová M., Květoa J., Vrábl D., Kubásek J., Macková J., Wiesnerová D., Neuwithová J. and Schreiber L. (2014) Stomatal and pavement cell density linked to leaf internal CO2 concentration. *Ann. Bot.* **114**, 191–202.

Schubert B. A. and Jahren A. H. (2012) The effect of atmospheric CO2 concentration on carbon isotope fractionation in C3 land plants. *Geochim. Cosmochim. Acta.* **96**, 29–43.

Seibt U., Rajabi A., Griffiths H. and Berry J. A. (2008) Carbon isotopes and water use efficiency: sense and sensitivity. *Oecologia* **155**, 441–454.

Smith F. A., Wing S. L. and Freeman K. H. (2007) Magnitude of the carbon isotope excursion at the Paleocene-Eocene thermal maximum: The role of plant community change. *Earth Planet. Sci. Lett.* **262**, 50–65.

Smith R. Y., Basinger J. F. and Greenwood D. R. (2009) Depositional setting, fossil flora, and paleoenvironment of the Early Eocene Falkland site, Okanagan Highlands, British Columbia. *Can. J. Earth Sci.* **46**, 811–822.

Smith R. Y., Basinger J. F. and Greenwood D. R. (2012) Early Eocene plant diversity and dynamics in the Falkland flora, Okanagan Highlands, British Columbia, Canada. *Palaeobiodiversity Palaeoenviron.* **92**, 309–328.

Tipple B. J., Meyers S. R. and Pagani M. (2010) Carbon isotope ratio of Cenozoic CO2: a comparative evaluation of available geochemical proxies. *Paleoceanography* **25**, 1–11.

Uhl D., Christofer T., Ursel G. and Thomas D. (2007) Fossil leaves as palaeoclimate proxies in the Palaeogene of Spitsbergen (Svalbard). *Acta Paleobot.* **47**, 89–107.

Vajda V. and Bercovici A. (2014) The global vegetation pattern across the Cretaceous – Paleogene mass extinction interval: a template for other extinction events. *Glob. Planet. Change* **122**, 29–49.

Voelker S. L., Brooks J. R., Meinzer F. C., Anderson R., Bader M. K. F., Battipaglia G., Becklin K. M., Beerling D., Bert D., Betancourt J. L., Dawson T. E., Domec J. C., Guyette R. P., Körner C., Leavitt S. W., Linder S., Marshall J. D., Mildner M., Ogée J., Panyushkina I., Plumpton H. J., Pregitzer K. S., Saurer M., Smith A. R., Siegwolf R. T. W., Stambaugh M. C., Talhelm A. F., Tardif J. C., Van de Water P. K., Ward J. K. and Wingate L. (2016) A dynamic leaf gas-exchange strategy is conserved in woody plants under changing ambient CO2: Evidence from carbon isotope discrimination in paleo and CO2 enrichment studies. *Glob. Chang. Biol.* 22, 889–902.

West C. K., Greenwood D. R. and Basinger J. F. (2015) Was the Arctic Eocene "rainforest" monsoonal? Estimates of seasonal precipitation from early Eocene megafloras from Ellesmere Island, Nunavut. *Earth Planet. Sci. Lett.* **427**, 18–30.

West C. K., Greenwood D. R. and Basinger J. F. (2019) The late Paleocene and early Eocene Arctic megaflora of Ellesmere and Axel Heiberg islands, Nunavut Canada. *Palaeontogr. Abt. B* **300**, 47–163.

Wilf P. and Johnson K. R. (2004) Land plant extinction at the end of the Cretaceous: a quantitative analysis of the North Dakota megafloral record. *Paleobiology* **30**, 347–368.

Wilf P., Johnson K. R. and Huber B. T. (2003) Correlated terrestrial and marine evidence for global climate changes before mass extinction at the Cretaceous – Paleogene boundary. *Proc. Natl. Acad. Sci. USA* **100**, 599–604.

Wilf P., Wing S. L., Greenwood D. R. and Greenwood C. L. (1998) Using fossil leaves as paleoprecipitation indicators: an Eocene example. *Geology* **26**, 203–206.

Willard D. A., Donders T. H., Reichgelt T., Greenwood D. R., Sangiorgi F., Peterse F., Nierop K. G. J., Frieling J., Schouten S. and Sluijs A. (2019) Arctic vegetation, temperature, and hydrology during Early Eocene transient global warming events. *Glob. Planet. Change* **178**, 139–152.

Wing S. L. (1987) Eocene and oligocene floras and vegetation of the rocky mountains. *Ann. Missouri Bot. Gard.* **74**, 748–784.

Wing S. L. and Boucher L. D. (1998) Ecological aspects of the Cretaceous flowering plant radiation. *Annu. Rev. Earth Planet. Sci.* **26**, 379–421.

Wing S. L. and Currano E. D. (2013) Plant response to a global greenhouse event 56 million years ago. *Am. J. Bot.* **100**, 1234–1254.

Wing S. L. and Greenwood D. R. (1993) Fossils and fossil climate: the case for equable continental interiors in the Eocene. *Philos. Trans. R. Soc. London B* **341**, 243–252.

Wing S. L., Strömberg C. A. E., Hickey L. J., Tiver F., Willis B., Burnham R. J. and Behrensmeyer A. K. (2012) Floral and environmental gradients on a Late Cretaceous landscape. *Ecol. Monogr.* **82**, 23–47.

Wolfe J. A. (1993) A method of obtaining climatic parameters from leaf assemblages. *United States Geol. Surv. Bull.* **2040**, 1–71.

Woodward F. I. (1987) Stomatal numbers are sensitive to increases in CO2 from pre-industrial levels. *Nature* **327**, 617–618.

Woodward F. I. and Kelly C. K. (1995) The influence of CO2 concentration on stomatal density. *New Phytol.* **131**, 311–327.

Wu M. S., Feakins S. J., Martin R. E., Shenkin A., Patrick L. P., Blonder B., Salinas N., Asner G. P. and Malhi Y. (2017) Altitude effect on leaf wax carbon isotopic composition in humid tropical forests. *Geochim. Cosmochim. Acta* **206**, 1–17.

Wullschleger S. D. (1993) Biochemical limitations to carbon assimilation in C_3 plants—a retrospective analysis of the A/C_i curves from 109 species. *J. Exp. Bot.* **44**, 907–920.

Yan W., Zhong Y. and Shangguan Z. (2017) Contrasting responses of leaf stomatal characteristics to climate change: a considerable challenge to predict carbon and water cycles. *Glob. Change. Biol.* **23**, 3781–3793.

Zaborac-Reed S. J. and Leopold E. B. (2016) Determining the paleoclimate and elevation of the late Eocene Florissant flora: support from the coexistence approach. *Can. J. Earth Sci.* **53**, 565–573.

Zachos J., Pagani H., Sloan L., Thomas E. and Billups K. (2001) Trends, rhythms, and aberrations in global climate 65 Ma to present. *Science* **292**, 686–693.

Zhang H. Y., Hartmann H., Gleixner G., Thoma M. and Schwab V. F. (2019) Carbon isotope fractionation including photosynthetic and post-photosynthetic processes in C3 plants: Low [CO2] matters. *Geochim. Cosmochim. Acta* **245**, 1–15.

Associate editor: Sarah J. Feakins